

## Author's response to comments by referee #1

We would like to thank the reviewer for his / her useful comments.

### *General Comments:*

*This paper presents near-surface and path-averaged mixing ratios of NO<sub>2</sub> derived from car DOAS zenith-sky and tower DOAS off-axis, measurements performed in Vienna city during several days on 2015 and 2016. This paper provides an useful intercomparison between tower DOAS, mobile DOAS and in-situ observations.*

### *Specific Comments:*

*Section 2 - Instrument and car journeys, in this section you should add few info about the in-situ instruments (type, error, etc.). Also please add a map (a new Figure) or include in Figure 1 the location of the in-situ monitoring stations and also the location of the DOAS tower instrument.*

We have now rewritten the first passage of Sect. 3.3 and added information about instrument type and error of in situ instruments. In addition, we now refer to a recently published report (Spangl, 2017) (see Page 14, Line12-20). In this report, which is available online, all the air quality monitoring stations are described in detail (e.g. instrument type, location, surrounding, etc.).

We have now indicated all in situ stations in Figure 1 that are used in combination with the car DOAS measurements, but also those that are used for comparison with tower DOAS measurements. We have now renounced to include the Table with all the station name/coordinates as this information about the in situ stations as even more details can be found in the mentioned report anyway. Also now shown in Figure 1 is the position of the Danube Tower, on which tower DOAS measurements were performed.

We have now included a sentence to describe what is seen in addition to the exemplary car route in this new Fig. 1 (see Page 8, Line 1-4).

*Please describe the tower DOAS instrument, I suggest you to introduce a Table with the technical characteristics of the two instruments (tower DOAS and mobile DOAS).*

The one and the same DOAS instrument, which we used for both car DOAS and tower DOAS applications, is already described in the version of the manuscript (see Sect. 2.1, 2.2, and 2.3 of the ACPD Manuscript Version). In order to provide more technical details of the DOAS instrument, we have now introduced a Table with the technical characteristics (see Table 1).

*Figure 2. Could you explain the very low peak of intensity? Is it related to a tree, tunnel, or a bridge? Did you filter all the DSCDs function of RMS and O<sub>4</sub>?*

The very low peak of intensity in Figure 2 is related to the tower DOAS measurements and shows up once every rotation of the tower platform, e.g. when the DC Tower (a skyscraper), which is about 1 km away from the Danube Tower, blocks the field of view of the instrument.

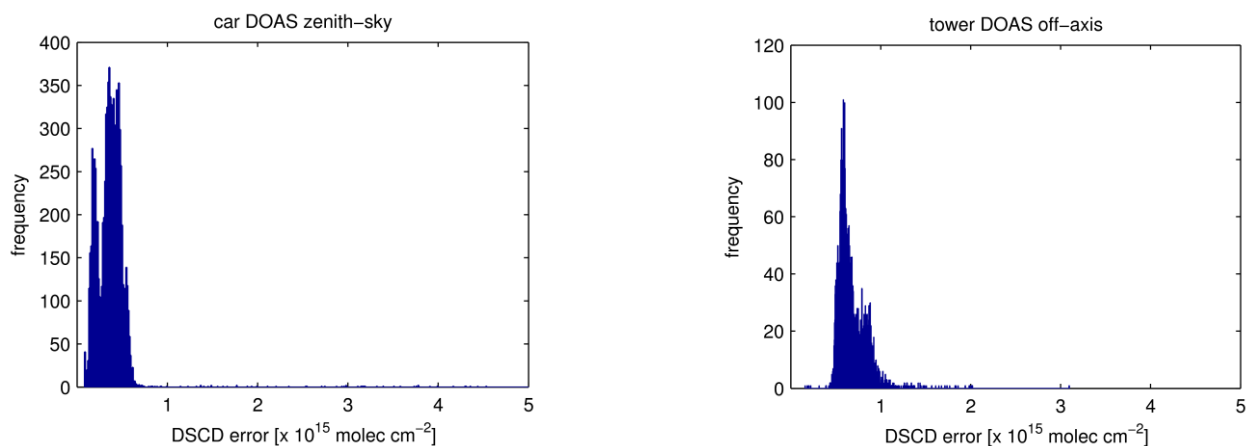
We have already described the reason for this low peak of intensity in the manuscript and used this peak for determining the exact orientation of the tower platform (see Page 8, Line 15-23 of the ACPD Manuscript Version).

For the car DOAS zenith-sky measurements, we filtered all the DSCDs as a function of chisquare, e.g. NO<sub>2</sub> DSCDs with chisquare values > 0.025 were not included in the analysis. This filtering is already described in the manuscript (see Page 9, Line 17-18 of the ACPD Manuscript Version). For the tower DOAS off-axis measurements, we did not apply any filtering.

We have now added a sentence mentioning that tower DOAS off-axis measurements are not filtered (see Page 10, Line 5-7).

*Figure 3, please introduce the DSCD error. Also please introduce the error of each DSCD presented in the manuscript.*

We have introduced and evaluated the error for each NO<sub>2</sub> DSCD presented in the manuscript. In general, the error of (unfiltered) DSCDs is lower than  $0.75 \times 10^{15}$  molec cm<sup>-2</sup> for car DOAS zenith-sky NO<sub>2</sub> DSCDs and lower than  $1.5 \times 10^{15}$  molec cm<sup>-2</sup> for tower DOAS off-axis NO<sub>2</sub> DSCDs presented in the manuscript (see Figures below).



We have now added a sentence to give an overall (maximum) error of NO<sub>2</sub> DSCDs for both car DOAS zenith-sky and tower DOAS off-axis measurements (see Page 10, Line 8-10).

*3.2.1 Temporal resolution and computation of horizontal NO<sub>2</sub> gradients- Could you specify the exposure time for the mobile DOAS instrument? (or this info could be included on the suggested Table for the two DOAS instrument).*

Typical values of the exposure time for car DOAS zenith-sky measurements were generally between 0.00625 and 0.1 seconds. In most cases, however, the exposure time was 0.025 seconds.

We have now added a sentence to specify the exposure time for the car DOAS zenith-sky measurements (see Page 10, Line 14-15 and also added this information in the new/additional Table 1.

### *3.2.2 Stratospheric NO<sub>2</sub> columns, Could you specify the error of Bremen 3d CTM (B3dCTM) model?*

It is difficult to quantify the accuracy of the stratospheric NO<sub>2</sub> columns from the Bremen 3d CTM. In absolute units, it is not very good as it is a free running model without data assimilation. However, in this analysis, the stratospheric model is only used for the diurnal cycle of the stratospheric NO<sub>2</sub> column as the absolute value is scaled to GOME2 satellite observations at the time of overpass. The uncertainty of the diurnal variation is large at twilight but small during the day as changes in stratospheric NO<sub>2</sub> are small when compared to tropospheric NO<sub>2</sub> columns in polluted regions. As a rough estimate, the uncertainty of the stratospheric correction is assumed to be less than 10% or typically  $1 \times 10^{15}$  molec cm<sup>-2</sup>.

We have now added a sentence to highlight the uncertainty in the stratospheric correction (see Page 12, Line 1-6).

*3.2.3 Conversion to tropospheric NO<sub>2</sub> vertical column densities SCDref, could you specify why you don't have a SCDref for each day? SCDref is quite important if you want to have qualitative data. I suggest to the authors to introduce more details about SCDref calculation, e.g. exact time of the selected SCDref. SCDref having  $1.3 \times 10^{15}$ ,  $1.1 \times 10^{15}$ , and  $2.2 \times 10^{15}$  molecules/cm<sup>2</sup> as tropospheric contribution could be realistic. Considering that SCDref contain stratospheric and tropospheric contributions, did you cancel the stratospheric contribution? why do you refer to SCDref as having only tropospheric contributions?*

We agree that it is important to have as many as possible SCDref measurements for quantitative data analysis. The reason why we didn't use SCDref of each single day in our study is that for most of the days, (noontime) SCDref was taken in urban areas, where pollution levels are expected to be higher. The three SCDref measurements that we used were recorded during noontime and outside of Vienna in rather rural areas, where pollution levels are expected to be low. According to Wagner et al. (2010), AMT, spatially inhomogeneous tropospheric trace gas concentrations are a prerequisite for the "zenith-sky only" approach to avoid large systematic errors when applying Eq. 11 in their paper (Eq. 1 in our ACPD Manuscript). By using SCDref measurements in areas with rather small tropospheric NO<sub>2</sub>, as we did in our study, the errors are kept as low as possible. The selection of the three SCDref measurements was a compromise between having such measurements during noontime in unpolluted regions and at the same time to keep the time difference between SCDref and the days for which these SCDref measurements are used as low as possible (< 9 days). There are other examples in the literature where only few SCDref measurements are used for similar DOAS-type analyses (e.g. Tack et al. 2015, AMT). The authors of that study use a single SCDref measurement for a period of about 40 days. Because a similar approach to convert zenith-sky DOAS measurements into tropospheric NO<sub>2</sub> vertical columns is described in the latter publication, we have now included this study in the references.

We have specified the exact time and also the location (lat/long) of the three SCDref measurements that we used for our data analysis in Table 2. In addition, we have now added the exact time, SZA, and location of the three SCDref measurements used in our study and also we have now added more infos about how we calculated SCDref in Sec. 3.2.4 (Page 13, Line 12-21).

In order to not confuse the reader, we have now avoided the use of "tropospheric" amounts in SCDref and replaced it with "residual" amounts in Sect. 3.2.4 and 3.3. This formulation was already used in the literature before (e.g. Tack et al., 2015, AMT).

*A chapter to describe the AMF calculation (using NO<sub>2</sub> profiles, albedo, geometry, PBL, etc.) is mandatory for this study, I suggest to the authors to use a table. Figure 6 should be part of this section and should include the AMF calculations for several days which are presented in this study.*

In response to the comments of both reviewers, we have re-evaluated the AMFs used in the study by adding a sensitivity study of AMF changes for realistic values of AOD, single scattering albedo and mixing height in Vienna. Based on the results we have decided to change the AMF used to values based on an intermediate scenario which according to our sensitivity study provides a good compromise. All other scenarios are well within 20% of these values. Therefore, we have re-calculated VCD<sub>tropo</sub> NO<sub>2</sub> in our study and plotted the respective figures again.

Both the sensitivity study and the description of the AMF used have been included in a new Section (Sect. 3.2.3, Page 12, Line 8-27) in the revised manuscript.

*The authors should give more details about the error calculation of tropospheric NO<sub>2</sub> VCD, or a section of errors would be more appropriate.*

Uncertainties in tropospheric VCDs are introduced by uncertainties in the quantities used in equation 1 of the manuscript. Assuming that the stratospheric AMF is well known, the uncertainties of DSCD<sub>meas</sub>, SCD<sub>ref</sub>, SCD<sub>strato</sub> and AMF<sub>tropo</sub> need to be considered:

$$\Delta VCD_{tropo} = VCD_{tropo} \sqrt{\frac{\Delta DSCD_{meas}^2 + \Delta SCD_{ref}^2 + \Delta SCD_{strato}^2}{SCD_{tropo}^2} + \frac{\Delta AMF_{tropo}^2}{AMF_{tropo}^2}}$$

Here, SCD<sub>tropo</sub> is the tropospheric slant column and SCD<sub>strato</sub> the stratospheric slant column. For a typical situation with

$$\Delta DSCD_{meas} = 2 * 10^{16} \text{ molec cm}^{-2}$$

$$\Delta SCD_{ref} = 2 * 10^{14} \text{ molec cm}^{-2}$$

$$\Delta SCD_{strato} = 1 * 10^{15} \text{ molec cm}^{-2}$$

$$SCD_{tropo} = 1 * 10^{16} \text{ molec cm}^{-2}$$

$$\frac{\Delta AMF_{tropo}}{AMF_{tropo}} = 0.2$$

an overall uncertainty of 25% is found, dominated by the assumed 20% uncertainty of the AMF. For situations approaching twilight, the absolute uncertainty of the stratospheric correction increases, and the relative uncertainty of the slant column can become the dominating error source. If the background measurement SCD<sub>ref</sub> cannot be taken in a clean region, then the absolute uncertainty on this quantity can become large and important for the overall uncertainty (see Wagner et al., 2010).

We have now added a paragraph in order to provide information on the overall uncertainty of VCD<sub>tropo</sub> in our study (see Page 13, Line 27-28; Page 14, Line 1-9).

## Author's response to comments by referee #2

We would like to thank the reviewer for his / her useful comments.

### *General comments:*

*The paper presents approaches to derive near-surface and path-averaged mixing ratios from zenith-sky car DOAS and azimuth tower DOAS observations as well as a comparison with mixing ratios derived from in situ monitoring stations. Based on 9 days of car DOAS measurements and 5 days of tower measurements, acquired in 2015 and 2016, the paper provides an insight on the NO<sub>2</sub> spatiotemporal distribution in Vienna, Austria.*

*The paper is well written and generally well-structured and provides interesting approaches to study the urban spatiotemporal NO<sub>2</sub> distribution. The paper has improved compared to the initial submission and most comments provided in the quick review are addressed well. However, some critical issues remain and therefore my opinion has not changed that the paper would better fit in the scope of AMT than ACP.*

*The work has a stronger focus on the performed measurement techniques and applied retrievals approaches than on geophysical interpretation of the data, chemical/physical processes and new findings on the urban spatiotemporal NO<sub>2</sub> distribution. I would support publication in ACP when more data and better statistics would be available in order to thoroughly assess the novel approaches and to substantiate the findings, e.g. based on long-term, routine tower DOAS and car DOAS measurements. The authors recognize the limited data set several times in the paper and foresee routine measurements based on tower DOAS off-axis and MAX-DOAS in the future.*

We agree that our manuscript might also fit in the scope of AMT. We do not fully agree with the argument that more data are needed to publish such a study in ACP. On the one hand, we have clearly defined our study as a "case study". On the other hand, there are other studies in ACP which evaluate data from only few days. "Estimation of NO<sub>x</sub> emissions from Delhi using Car MAX-DOAS observations and comparison with OMI satellite data" by Shaignafar et al. (2011), a well cited ACP study, is only one example.

*A new, and indeed interesting, approach to convert DOAS columns to near-surface VMR (a very relevant but complex problem!) based on a linear regression analysis is introduced but not developed well in the paper. This is something that the authors recognize and attribute to the limited data/statistics available. Most of the analysis in 4.3 (comparison of car-DOAS with in-situ measurements) is not based on the new approach but on a simple assumption, assuming a constant mixing ratio in the BLH. The authors discuss that this is not necessarily valid in an urban area. I fully agree with this and I highly doubt the validity of this approach in a city, where you rather expect an exponential NO<sub>2</sub> profile and also a strong variability over city, industry and highways. The data set is too small to fully evaluate the approach and some correlations are bad which is most likely related to the wrong assumptions in the NO<sub>2</sub> vertical distribution. If the authors keep this approach in the paper they should at least assess the impact of other, more realistic, NO<sub>2</sub> profiles on the statistical comparison with in situ stations and perform a sensitivity study. Eventually typical urban NO<sub>2</sub> profiles could be derived from a high resolution CTM.*

We agree that the newly introduced linear regression analysis is not yet developed well, which mainly depends on the availability of data for only few days. Nevertheless, we argue that it is meaningful to present a new method to convert VCD<sub>tropo</sub> into near-surface mixing ratios, even if only limited data is available. The collection of data, which is available for testing this new method, was well thought out and a lot of effort and time was spent to get this unique data set. There is no comparable study, which collected data for one and the same car route for many times as well as for many different meteorological conditions. We argue that our data, collected in an urban environment, in combination with a relatively large number of air quality monitoring stations, is exactly what we need for introducing and testing such a new method.

We agree that most of the analysis in Sect. 4.3 is based on the method of Knepp et al. (2013). From this analysis we found that for some days (mostly when air masses came from southeastern directions and when wind speeds were rather low) the correlation was high but slope and intercept were not satisfying enough, most probably because of the fact that the assumption of a constant mixing ratio within the PBL does not work for urban environments having different meteorological conditions. Again, our intention was to perform such car DOAS zenith-sky measurements on days with different meteorological conditions to see how these changing conditions affect the assumption of a constant mixing ratio within the PBL. The findings of this analysis raised the motivation to go one step further and test a new method – a method that seems to reduce the complexity of the problem of converting DOAS columns to near-surface mixing ratios, without deriving typical NO<sub>2</sub> profiles from highly resolved CTM, which also have well known problems in representing the vertical distribution of NO<sub>2</sub> in complex urban environments. Our aim was not to fully evaluate this method but rather introduce it and test it on a unique data set.

We agree that deriving typical urban profiles from high resolution CTMs and perform sensitivity analysis to assess the impact of more realistic NO<sub>2</sub> profiles is an interesting and worthwhile suggestion. However, the main motivation of this work was to evaluate a new method, and as shown in Fig. 17, this method appears to perform very well for at least for our data set.

*Specific comments:*

*P3, L9: The background signal in the reference could also be obtained by measuring one additional spectrum at 30° at the reference area and by application of the geometric approximation approach.*

We agree that additional measurements at EA = 30° would help in this case. Unfortunately, such measurements were not performed and are thus not available. Nevertheless, we will consider such measurements for future car DOAS measurements.

*P10, L13: Please quantify improvement in SNR after averaging + same for averaging tower measurement on P16, L17.*

It is not clear to us what the reviewer would like to see here. Averaging reduces the variability in NO<sub>2</sub> signal as expected, and this is illustrated in Figure 4 in the manuscript. Raw data (0.05 seconds) appear to have a random scatter of the order of  $8 \times 10^{15}$  molec cm<sup>-2</sup> peak-to-peak, which is reduced to less than  $1 \times 10^{15}$  molec cm<sup>-2</sup> in the averaged data (5 seconds). Thus one could say that the signal to noise ratio has improved by a factor of 8. However, as also seen in Fig. 4, it is not trivial to distinguish between measurement related noise and real atmospheric variability, and thus it is in our opinion not clear what the real improvement in SNR is.

*P26, L3: I would elaborate a bit more on the comparison between tower VMR (at 160 m) and in-situ station VMR as this is indicated as novel in the introduction, e.g. by quantifying both instead of only giving an overall factor.*

Due to the fact that data is only available for a couple of days, and reasonable comparison between tower and in situ NO<sub>2</sub> mixing ratios can only be made for the two rotations of 29 April and 9 May 2016, quantification is challenging. Nevertheless, we have now added a new figure (Fig. 21) to compare the NO<sub>2</sub> mixing ratios derived from tower DOAS off-axis measurements with the one calculated from surface NO<sub>2</sub> concentrations. The comparison is based on round 4 and round 6 of 29 April and 9 May 2016, respectively (e.g. the same two rounds as presented in Fig. 18, Fig. 19, and Fig. 20). We have computed the mean and standard deviation of tower DOAS off-axis NO<sub>2</sub> mixing ratios of the full tower rotation and the mean and standard deviation of in situ NO<sub>2</sub> mixing ratios from those stations which are within the circle as determined by hOPL. The results are described in Sect. 4.5 (Page 29, Line 1-18) and Sect. 5 (Page 31, Line 23-24) and highlighted in the abstract.

*P20, L18: Please give a number on how far the air masses moved based on wind speed and time difference between the measurements. This allows to cross-check if indeed the same air masses are observed.*

When considering round-averaged wind directions, wind speeds and 1.5 hours for the time difference between the measurements at one and the same location, air masses on 10 April 2015 moved about 5.85 km (from the first to the second round) and 8.1 km (from the second to the third round). Consequently, in total those air masses moved about 14 km, which is in good agreement with the position of the NO<sub>2</sub> peak of round 1 (red) at about 20 km and the position of the second of the two NO<sub>2</sub> peaks of round 3 (blue) at about 6 km (see Fig. 11). We note that the 3-rounds averaged wind direction of that day (125.3 deg) slightly differs from the position of the A22 highway (~150 deg), which was considered for this case study.

*P24, L4: As indicated earlier, weak correlations are probably related due to wrong assumptions in the NO<sub>2</sub> profile.*

We agree that weak correlations are probably related due to wrong assumptions in the NO<sub>2</sub> profile, in addition to changing air masses with sometimes only low pollution levels. As argued above, we conclude that using the method of Knepp et al. (2013) assuming constant mixing of NO<sub>2</sub> within the PBL does not work as good for all days of our study performed in the urban environment of Vienna. This fact was basically the motivation to test a new method, e.g. the linear regression analysis, which also accounts for other meteorological parameters that could have an effect on NO<sub>2</sub> profiles, e.g. wind speed. Due to the good correlation between modeled and measured NO<sub>2</sub> surface mixing ratios ( $R = 0.94$ ) achieved with this new introduced and tested method we can argue that NO<sub>2</sub> profiles are not essentially needed for the conversion of VCD<sub>tropo</sub> into mixing ratios as wind speed, na, MH seem to strongly affect NO<sub>2</sub> profiles, at least over the urban area of Vienna, and at least for the data we have analyzed. This is generally the main message of our introduced and tested method. In the future, we will apply this method to zenith-sky measurements from operating MAX-DOAS instruments in Vienna, where better statistics are available. While weak correlation is found when using the method of Knepp et al. (2013), a very high correlation is found with our new method. This makes it worthwhile enough to publish this method and

to motivate other research group to work on this complex problem of converting DOAS columns to surface mixing ratios.

*Technical corrections:*

*P3, L9: great advantage < added-value*

*P4, L9: add "for example" after estimated*

*P8, L12: rotations < rotation*

*P10, L10: drives < route*

*P10, L11: lines < box*

*P11, L26: the < an*

*P15, L4: In situ < in situ*

*P19, L5: move "are" behind "magnitude"*

We have considered all the "technical corrections" in the new version of the manuscript.

*P19, L16: Is "temporal evolution" appropriate in the title, as you also measure spatial distribution with the moving measurement platform? Maybe split as well the car and tower measurements in different (sub)sections as they are not directly linked.*

We agree that "temporal evolution" is not meaningful enough in this case and thus, changed it into "spatio-temporal patterns" (see Page 21, Line 22-23). We also agree that for a better overview, splitting car and tower DOAS (Sect. 4.2) is the right way. We have now added a new (sub)section (Sect. 4.3) (see Page 23, Line 21-22). We have now also added "obtained from tower DOAS off-axis" in the title of Sect. 4.5 (see Page 27, Line 12).

*P26, L22: "unique" is not appropriate*

We have now removed "unique" in the first sentence of the summary and outlook sections.

*P46 – Figure3: Please put residuals on another scale. It is not possible to check potential residual structures at this scale*

We have now put residuals on a different scale to make them more readable (see Page 51).



1 **Near-surface and path-averaged mixing ratios of NO<sub>2</sub> derived**  
2 **from car DOAS zenith-sky and tower DOAS off-axis**  
3 **measurements in Vienna: a case study**

4 **Stefan F. Schreier<sup>1</sup>, Andreas Richter<sup>2</sup>, and John P. Burrows<sup>2</sup>**

5 <sup>1</sup>Institute of Meteorology, University of Natural Resources and Life Sciences, Vienna, Austria

6 <sup>2</sup>Institute of Environmental Physics, University of Bremen, Germany

7 Correspondence to: S. F. Schreier (stefan.schreier@boku.ac.at)

8

9

10 **Abstract.** Nitrogen dioxide (NO<sub>2</sub>), produced as a result of fossil fuel combustion, biomass burning,  
11 lightning, and soil emissions, is a key urban and rural tropospheric pollutant. In this case study,  
12 ground-based remote sensing has been coupled with the in situ network in Vienna, Austria, to  
13 investigate NO<sub>2</sub> distributions in the planetary boundary layer. Near-surface and path-averaged NO<sub>2</sub>  
14 mixing ratios within the metropolitan area of Vienna are estimated from car DOAS (Differential  
15 Optical Absorption Spectroscopy) zenith-sky and tower DOAS horizon observations. The latter  
16 configuration is innovative in the sense that it obtains horizontal measurements at more than  
17 hundred different azimuthal angles – within a 360° rotation taking less than half an hour. Spectral  
18 measurements were made with a DOAS instrument on nine days in April, September, October, and  
19 November 2015 in the zenith-sky mode and on five days in April and May 2016 in the off-axis  
20 mode. The analysis of tropospheric NO<sub>2</sub> columns from the car measurements and O<sub>4</sub> normalized  
21 NO<sub>2</sub> path averages from the tower observations provide interesting insights into the spatial and  
22 temporal NO<sub>2</sub> distribution over Vienna. Integrated column amounts of NO<sub>2</sub> from both DOAS-type  
23 measurements are converted into mixing ratios by different methods. The estimation of near-  
24 surface NO<sub>2</sub> mixing ratios from car DOAS tropospheric NO<sub>2</sub> vertical columns is based on a linear  
25 regression analysis including mixing-height and other meteorological parameters that affect the  
26 dilution and reactivity in the planetary boundary layer – a new approach for such conversion. Path-

Formatte

1 averaged NO<sub>2</sub> mixing ratios are calculated from tower DOAS NO<sub>2</sub> slant column densities by taking  
2 into account topography and geometry. Overall, lap averages of near-surface NO<sub>2</sub> mixing ratios  
3 obtained from car DOAS zenith-sky measurements, around a circuit in Vienna, are in the range of  
4 3.8 to 26.21 ppb and in good agreement with values obtained from in situ NO<sub>2</sub> measurements ~~for~~  
5 ~~days with wind from the Southeast.~~(R = 0.94). Path-averaged NO<sub>2</sub> mixing ratios at 160 m above  
6 the ground as derived from the tower DOAS measurements are between 2.5 and 9 ppb on two  
7 selected days with different wind conditions and ~~pollution levels and show similar spatial~~  
8 ~~distribution as seen in the car DOAS zenith-sky observations.~~are about a factor 6.5 smaller than  
9 NO<sub>2</sub> mixing ratios derived from surface in situ stations. We conclude that the application of the  
10 two methods to obtain near-surface and path-averaged NO<sub>2</sub> mixing ratios is promising for this case  
11 study.

12

## 13 **1 Introduction**

14 Tropospheric nitrogen oxides (NO<sub>x</sub> = NO + NO<sub>2</sub>) are released from various human activities and  
15 natural sources (Lee et al., 1997). Fossil fuel combustion to produce energy results in NO<sub>x</sub>  
16 emissions by traffic, industry and domestic heating or cooling appliances. Nitric oxide (NO) is the  
17 predominant part of NO<sub>x</sub> emitted from these sources. However, it is rapidly converted to nitrogen  
18 dioxide (NO<sub>2</sub>) by reaction with ozone (O<sub>3</sub>). During daytime, given sufficient ultraviolet radiation,  
19 NO<sub>2</sub> is photolysed to produce NO and oxygen atoms. The reaction of oxygen atoms with molecular  
20 oxygen (O<sub>2</sub>) results in the production of O<sub>3</sub>. Under polluted conditions, the so called Leighton  
21 photostationary state is established. However, as the NO<sub>x</sub> air is mixed in daylight with  
22 hydrocarbons and being diluted, the catalytic production of O<sub>3</sub> results and nitric acid (HNO<sub>3</sub>) is  
23 formed. The latter is absorbed on aerosols, which are also produced in air masses generating  
24 photochemical smog.

25 Although NO<sub>x</sub> concentrations are relatively low in the atmosphere, these reactive gases play a  
26 significant role in atmospheric chemistry, air pollution, and climate change, in particular in urban  
27 environments (e.g. WHO, 2003; IPCC, 2013). For example, elevated levels of air pollutants such  
28 as NO<sub>2</sub> and O<sub>3</sub> affect human health (e.g. Dockery et al., 1993), as the long-term exposure to these  
29 gases can influence mortality and morbidity (e.g. Künzli et al., 2000).

1 In addition to the in situ NO<sub>2</sub> measurement techniques such as chemiluminescence monitors (e.g.  
2 Fontijn et al., 1970), the differential optical absorption spectroscopy (DOAS) method (Perner and  
3 Platt, 1979) can also be used to quantify atmospheric NO<sub>2</sub> concentrations. Nowadays, the DOAS  
4 technique is a widely-used remote sensing method to retrieve the amount of several trace gases  
5 having narrow band absorption structures in the UV and visible part of the electromagnetic  
6 spectrum. The (passive) DOAS principle, which is based on Lambert-Beer's law, can be applied to  
7 measurements from various ground-based, ship-based, aircraft-based, and satellite-based platforms  
8 (e.g. Platt and Stutz, 2008 and references therein).

9 The ~~great advantage~~added-value of satellite-based measurements is their daily (near) global  
10 coverage and thus, the possibility to evaluate temporal trends above selected regions. However, it  
11 is difficult to resolve NO<sub>2</sub> at the city scale because of the coarse resolution of satellite sensors  
12 (Richter et al., 2005; Hilboll et al., 2013). Aircraft-based measurements deliver higher resolved  
13 images of the spatial NO<sub>2</sub> distribution along a given flight track, but only during short-term  
14 measurement campaigns (Heue et al., 2005; Wang et al., 2005; Schönhardt et al., 2015; Meier et  
15 al., 2017; Nowlan et al., 2018). As is the case for aircraft-based DOAS measurements of NO<sub>2</sub>, ship-  
16 based observations of NO<sub>2</sub> are also usually performed on a campaign basis (Peters et al., 2012;  
17 Takashima et al., 2012; Schreier et al., 2015; Hong et al., 2018). Finally, information on  
18 tropospheric NO<sub>2</sub> can also be obtained from ground-based platforms using the Multi AXis (MAX)  
19 DOAS system (Hönninger et al., 2004; Wittrock et al., 2004). In contrast to other platforms,  
20 ground-based DOAS measurements are usually performed continuously and at fixed locations.

21 More recently, DOAS-type measurements of NO<sub>2</sub> are also performed from a car, which enables  
22 the observation of the horizontal variation of tropospheric NO<sub>2</sub>, in addition to its temporal  
23 evolution. Such observations have been used for the quantification of total emissions from cities  
24 and/or known emission sources (Johansson et al., 2008; Rivera et al., 2009; Ibrahim et al., 2010;  
25 Shaiganfar et al., 2011; Wang et al., 2012; Frins et al., 2014; Ionov et al., 2015), for the estimation  
26 of emission fluxes from cities (Johansson et al., 2009; Rivera et al., 2013), for the comparison with  
27 satellite observations of NO<sub>2</sub> (Wagner et al., 2010; Constantin et al., 2013; Wu et al., 2013), for the  
28 comparison with model simulations (Dragomir et al., 2015), and for the validation of airborne  
29 measurements of NO<sub>2</sub> (Meier et al., 2017; Tack et al., 2017; Merlaud et al., 2018). While some of  
30 the mentioned studies use the MAX-DOAS measurement principle, others apply their instruments

1 in the zenith-sky viewing mode only. The main challenges for the retrieval of tropospheric NO<sub>2</sub> for  
2 the latter approach are obtaining accurate knowledge of the NO<sub>2</sub> signal in the reference  
3 measurement as well as the removal of the stratospheric NO<sub>2</sub> contribution (as a function of SZA).  
4 Both quantities cannot directly be separated from the zenith-sky measurements alone and thus, not  
5 accounting for these contributions can lead to large errors, especially in regions with low NO<sub>2</sub>  
6 levels (Wagner et al. 2010). Therefore, approaches were developed to estimate these contributions  
7 by using additional data and methods. While the stratospheric NO<sub>2</sub> amounts can be obtained from  
8 satellite measurements in combination with atmospheric modelling, the background signal in the  
9 reference spectrum can be estimated, for example, by calculating a reference measurement  
10 applying the Langley-plot method (Constantin et al. 2013). Another approach to estimate the  
11 background signal in the reference spectrum would be to utilize NO<sub>2</sub> concentration measurements  
12 from nearby in situ monitoring stations and convert those quantities into tropospheric NO<sub>2</sub> vertical  
13 columns, e.g. by applying an empirical relationship (Kramer et al., 2008).

14 The aims of the present study are two-fold. Firstly, it attempts to build on earlier work and  
15 investigates the spatial and temporal variability of NO<sub>2</sub> pollution in Vienna by using a simple  
16 zenith-sky telescope and a miniature spectrometer operated from a normal car. The relatively large  
17 number of air quality monitoring stations in and around Vienna, including continuous  
18 measurements of NO<sub>2</sub> concentrations at the surface level, provides the prerequisites for a  
19 comparison between these two observation systems, which has not yet been performed in past  
20 studies. Secondly, the potential of DOAS horizon measurements, performed with the same  
21 instrument on a rotating tower platform in Vienna is investigated – a DOAS-type approach to gain  
22 detailed horizontal NO<sub>2</sub> distributions on the city-scale within less than half an hour. Our tower  
23 DOAS off-axis observations can be best compared to the measurement configuration of the CU 2-  
24 D-MAX-DOAS instrument during the Multi-Axis DOAS Comparison campaign for Aerosols and  
25 Trace gases (MAD-CAT) in Mainz, Germany (Ortega et al., 2015). The authors of that study  
26 developed a four-step retrieval to derive, amongst other parameters, near-surface horizontal  
27 distributions of NO<sub>2</sub> at 14 pre-set azimuth angles distributed over a 360° view. The tower DOAS  
28 off-axis configuration presented in our study is in the sense innovative that it is the first approach  
29 having more than 100 horizontal measurements within a 360° rotation that lasts less than half an  
30 hour. Also new is the performance of the DOAS instrument at an altitude of more than 100 meters

1 above ground, which gives insights into the vertical variability of NO<sub>2</sub> within the planetary  
2 boundary layer over the urban environment of Vienna, when these measurements are combined  
3 with ground-based in situ data. The horizontal optical path lengths in our study are estimated by  
4 making use of the combination of geometry and topography. We note that the discussion of tower  
5 DOAS off-axis measurements is only based on a couple of data available. Further measurements  
6 on a routine base could serve as a data set to go more in detail and estimate the 3-D distribution of  
7 trace gases, as shown in Ortega et al. (2015).

8 From both DOAS-type columnar NO<sub>2</sub> measurements reported in our study, near-surface and path-  
9 averaged NO<sub>2</sub> mixing ratios are estimated by using both existing methods and a novel linear  
10 regression analysis. These measurements provide insights about the NO<sub>2</sub> distributions in the  
11 Viennese boundary layer, which are interestingly in themselves but could also help in deciding  
12 where to place an optimal set of MAX-DOAS instruments around the capital and largest city of  
13 Austria. The proposed long-term measurements of ~~thesesuch~~ instruments, which are foreseen in  
14 the VINDOBONA (VIenna horizontal aNd vertical Distribution OBServations Of Nitrogen dioxide  
15 and Aerosols) project ([www.doas-vindobona.at](http://www.doas-vindobona.at)), will provide a valuable data set for analyzing the  
16 temporal variability of air pollutants over Vienna.

17 The city of Vienna has the second largest number of inhabitants (about 1.8 million) within German  
18 speaking countries. It is part of a metropolitan area having a population of 2.8 million and is a  
19 typical example of a growing city ([www.statistik.at](http://www.statistik.at)). There are many NO<sub>x</sub> emission sources such  
20 as high-traffic roads, individual power plants, and industrial buildings that contribute to increased  
21 levels of NO<sub>2</sub>. The Environment Agency Austria reported a significant decrease in NO<sub>x</sub> emissions  
22 from traffic and industry since 2005 in Austria, which is mainly because of the progress in  
23 automotive technology. However, they also highlighted the fact that a defined legal limit of annual  
24 mean NO<sub>2</sub> concentrations (35 µg/m<sup>3</sup>) was still exceeded in the past years at several Austrian air  
25 quality monitoring stations – including stations in Vienna (Spangl and Nagl, 2016). In the year  
26 2015, annual mean NO<sub>2</sub> concentrations exceeded the legal limit at one station in Vienna. Moreover,  
27 hourly limit values (200 µg/m<sup>3</sup>) were exceeded several times at four stations. We note that NO<sub>2</sub>  
28 levels didn't exceed the legal limits on the days of measurements presented in this case study.  
29 However, a substantial number of hourly values with NO<sub>2</sub> concentrations higher than 100 µg/m<sup>3</sup>  
30 were observed on these days.

1 In the following Sect. 2, the DOAS instrument and the setups for the car DOAS zenith-sky and  
2 tower DOAS off-axis measurements are introduced. Details about the data analysis, including the  
3 retrieval of columnar tropospheric NO<sub>2</sub> amounts and the conversion into mixing ratios are given in  
4 Sect. 3. The results of this study are described and discussed in Sect. 4, followed by a short  
5 summary and outlook (Sect. 5).

6

## 7 **2 Instrument and car journeys**

### 8 **2.1 DOAS instrument**

9 For the car DOAS zenith-sky and tower DOAS off-axis observations of tropospheric NO<sub>2</sub> in  
10 Vienna, a DOAS system was used to measure scattered sunlight from directly overhead and from  
11 the horizon, respectively. A cardboard box was built to house a commercial Avantes miniature  
12 spectrometer (AvaSpec-ULS2048x64) and a notebook. The AvaSpec-ULS2048x64 is small in size  
13 (175 x 110 x 44 mm), robust, and lightweight (855 grams). The instrument performs spectral  
14 measurements between 290 and 550 nm at a spectral resolution of 0.65 nm- (see [Table 1](#)). Both the  
15 spectrometer and notebook where supplied with electricity from the car battery and from the  
16 existing tower power circuit during the measurements.

17

### 18 **2.2 Setup of the car DOAS zenith-sky measurements**

19 An optical fibre was connected to the spectrometer and threaded through an aluminium bracket to  
20 the outside of the car, where it was fixed to a small aluminium plate by duct tape. In order to prevent  
21 direct sunlight from entering the optical fibre, a cylindrical plastic tube was used for shading the  
22 entrance. The field of view of the optical fibre was characterized in the laboratory to be about  $\pm 5^\circ$ .  
23 As the telescope was directed to the zenith, no large errors are expected for the retrieval of  
24 tropospheric vertical NO<sub>2</sub> columns in this case as light path length is relatively insensitive to small  
25 deviations of the pointing from the zenith direction. For stability reasons, the bracket was clamped  
26 by the two door windows of the rear area. The geographical position of the car was recorded by a  
27 GPS receiver, which was connected to and powered by a USB port of the laptop computer.

1 The overall approach was to keep the measurement system simple. Therefore, only the zenith-  
2 direction was implemented, which is insensitive to changes in pointing as from telescope  
3 misalignments or car movements. Pointing the instrument closer to the horizon increases the  
4 sensitivity to tropospheric NO<sub>2</sub>, but introduces additional complication as pointing accuracy in a  
5 moving car becomes an issue. Experience also showed that in a city environment, a large fraction  
6 of the measurements at 22° or 30° elevation, for example, is affected by blocking from houses,  
7 trees or other vehicles. As shown in previous studies (e.g. Wagner et al., 2010; Shaiganfar et al.,  
8 2011), the air mass factor for measurements at 22° and 30° depends on the relative azimuth between  
9 the telescope orientation and the sun, necessitating computation of the car heading from GPS data  
10 which can be complex in typical city traffic situations. In summary, the choice was made to use a  
11 simple and robust method at the expense of reduced sensitivity.

12 A total of twenty identical car circuits around Vienna were performed on nine days in April,  
13 September, October, and November 2015 within the metropolitan area of Vienna (see Table 23).  
14 Each drive spanned about 110 km and lasted about 1.5 hours. In order to minimize the effect of  
15 clouds and wind speed, measurements were performed in the morning rather than in the afternoon.  
16 After a successful test phase of the car DOAS zenith-sky measurements on 10 April 2015, more  
17 days were planned in fall of the same year, including working days and days on weekends as well  
18 as days with different wind conditions. Measurements between April and September, e.g. during  
19 the summer season, were unfortunately not possible due to other priorities and due the fact that the  
20 authors were not located in Vienna during that time.

21 Figure 1 illustrates an exemplary overview of a single car journey performed on 10 April 2015  
22 between 5:27 and 6:59 UT. The starting point of each drive was within the Municipality of  
23 Wolkersdorf im Weinviertel (48° 22' 59'' N, 16° 31' 05'' E), a small city located in Lower Austria,  
24 about 10 km north of Vienna and away from large sources of NO<sub>x</sub>. From there, the journey was  
25 planned to cover one of the busiest motorways in Austria, pass by known emission sources (e.g.  
26 power plants), and drive round one of the largest inland refineries in Europe, before heading back  
27 to the starting point on a different route. Also shown in Fig.1 are the air quality monitoring stations  
28 that are used for comparison purposes (see Sect. 3.3) as well as the location of the Danube Tower,  
29 from which horizon measurements were performed (see the following Sect. 2.3).

1

## 2 **2.3 Setup of tower DOAS off-axis measurements**

3 The same DOAS instrument was used for the measurements performed from the Café at the Vienna  
4 Danube Tower (48° 14' 25" N, 16° 24' 36" E), which is rotating at about 160 m above ground  
5 (www.donauturm.at). Due to its geographical location (about 4.5 km to the northeast of the city  
6 center), it is possible to scan both urban and rural areas during a single anti-clockwise 360° rotation  
7 (duration = 26.5 minutes). In contrast to the car DOAS zenith-sky measurements (see Sect. 2.2),  
8 the telescope was directed towards the horizon at an elevation angle of 0°. An optical lens was  
9 placed in front of the light fibre entrance to reduce the field of view of the instrument to about 0.8°.  
10 Both the lens and the entrance of the optical fibre were protected from direct sunlight by a purpose-  
11 built cardboard. Because the scattered sunlight was passing through a thick glass window, no UV  
12 spectra could be recorded by the DOAS instrument from the rotating tower platform.

13 Tower DOAS off-axis observations were performed on five days in April and May 2016. More  
14 than thirty 360° scans of Vienna were recorded, each of them for an individual ~~rotations~~rotation of  
15 the Cafe. For reasons of simplicity and accessibility, zenith-sky measurements were only taken  
16 afterwards from the open terrace, which is located a few meters below.

17 As the Vienna Danube Tower does not provide information on the exact orientation of the platform,  
18 and due to the fact that the signal of the GPS receiver was not accurate enough to reliably determine  
19 the position along the circle, the horizontal viewing angle was determined by the following  
20 approach: The DC Tower 1, the tallest skyscraper in Austria, which is located in about 1 km  
21 distance from the Vienna Danube Tower, comes into field of view once every rotation and  
22 considerably reduces the signal (see Fig. 2). According to Google Earth, the position of the Vienna  
23 Danube Tower relative to this skyscraper is 167° (nearly south). By assuming that the rotation  
24 speed and the alignment on intensity minima are constant, the horizontal viewing angle can be  
25 determined from the periodic sharp reduction in intensity.

26

## 27 **3 Data analysis**



### 1 3.1 DOAS analysis

2 The spectral measurements as obtained during the individual car journeys and tower platform  
3 rotations are analyzed using the DOAS technique applying a nonlinear least-squares fitting  
4 algorithm. The spectral retrieval of NO<sub>2</sub> differential slant column densities (DSCDs) is based on a  
5 fitting window between 425 and 490 nm, a polynomial degree of five (car DOAS zenith-sky) and  
6 seven (tower DOAS off-axis), and a wavelength calibration using data from the Solar atlas of  
7 Kurucz et al., (1984). These general settings have been commonly used in recent studies for the  
8 retrieval of NO<sub>2</sub> DSCDs from ground-based DOAS-type measurements (e.g. Roscoe et al., 2010).  
9 High resolution absorption cross-sections of O<sub>3</sub>, NO<sub>2</sub>, O<sub>4</sub>, H<sub>2</sub>O, and a pseudo-cross section  
10 accounting for rotational Raman scattering as computed with QDOAS (Danckert et al., 2015) have  
11 been included in the two retrieval settings (see Table 42). The motivation for using a higher  
12 polynomial degree in the analysis of the horizon measurements are large broadband residuals found  
13 in the data. These residuals are attributed to the fact that the horizon measurements were taken  
14 through thick multi-layer glass while the zenith-sky measurement was taken outdoors.

15 Exemplary car DOAS zenith-sky fit results, recorded on 10 April 2015 (SZA = 47.68°) under  
16 elevated NO<sub>2</sub> pollution (DSCD = 4.02 x 10<sup>16</sup> molec cm<sup>-2</sup>), are shown in Fig. 3 (left panels). In some  
17 parts of the route, the zenith view of the instrument is obstructed by tunnels, bridges or other  
18 objects. These measurements were identified using an intensity criterion and removed from the  
19 data set. However, some outliers having unrealistically high values of NO<sub>2</sub> are still present in the  
20 data set, which strongly correlate with exceptional high chi-square values. Consequently, we only  
21 consider NO<sub>2</sub> DSCDs with chi-square values < 2.5 x 10<sup>-3</sup> for further analysis. Noontime  
22 measurements of three selected days, taken in rural areas and close to air quality monitoring stations  
23 are used as reference measurements (see Sect. 3.2.34 and Table 23).

24 Exemplary tower DOAS off-axis fit results obtained from a spectra recorded on 29 April 2016  
25 (SZA = 66.99°) under elevated NO<sub>2</sub> pollution (DSCD = 1.46 x 10<sup>17</sup> molec cm<sup>-2</sup>) are shown in Fig.  
26 3 (right panels). When comparing the two fit results, it becomes clear that the absorption by NO<sub>2</sub>  
27 in the horizontal path is larger by a factor of 3.6 in this case. This is because most of the NO<sub>2</sub> in  
28 urban environments is found in the boundary layer, close to the ground. In contrast, to the car

1 DOAS zenith-sky measurements, no filtering was applied to the tower DOAS off-axis  
2 measurements.

3 The uncertainty of the retrieved unfiltered NO<sub>2</sub> DSCDs was calculated from the fit. For car DOAS  
4 zenith-sky and tower DOAS off-axis measurements, this error is generally less than  $0.75 \times 10^{15}$   
5 molec cm<sup>-2</sup> and  $1.5 \times 10^{15}$  molec cm<sup>-2</sup>, respectively

## 7 **3.2 Car DOAS measurements of tropospheric NO<sub>2</sub>**

### 8 **3.2.1 Temporal resolution and computation of horizontal NO<sub>2</sub> gradients**

9 Typical exposure times for the car DOAS zenith-sky measurements were in the range of 0.00625  
10 to 0.1 seconds. In most cases, however, the exposure time was 0.025 seconds. In order to obtain  
11 some information about the signal to noise ratio of the instrument and the horizontal gradients of  
12 NO<sub>2</sub> present in the city, the temporal resolution of the car DOAS zenith-sky measurements was  
13 initially set to 0.505 seconds. The collected spectra were then averaged over intervals of 5 seconds  
14 (see Fig. 4), which corresponds to a traveled distance of about 100 m. An averaging interval of 5  
15 seconds was also used by Constantin et al. (2013) for their mobile measurements. ▲

16 The upper panel in Fig. 4 shows the temporal evolution of NO<sub>2</sub> DSCDs on 3 November 2015. The  
17 red and blue lines represent the full resolution of 0.5 seconds and averaged values, respectively.  
18 While the full resolution is noisy (maximum deviation  $\sim 5 \times 10^{15}$  molec cm<sup>-2</sup>), the averaged values  
19 follow the general pattern of NO<sub>2</sub> along the car ~~drives~~route. For better clarity, the middle panel  
20 illustrates a shorter section of that day, indicated by the green ~~lines~~box in the upper panel. The  
21 same is true for the lower panel, which represents a short section of the middle panel. Based on  
22 these results we argue that the selection of 5 seconds as an averaging interval appears to be optimal  
23 and a good compromise in our study, in spite of more information being found in the high-  
24 frequency data in some cases.

25 In addition to mapping the spatial distribution of NO<sub>2</sub> in Vienna, it is also interesting to evaluate  
26 typical horizontal gradients within the city. The identification of such mean horizontal gradients of  
27 NO<sub>2</sub> along the individual car routes is based on the following approach. Firstly, horizontal distances

1 between start and end point of individual car DOAS zenith-sky measurements at the full resolution  
2 of 0.505 seconds are calculated and summed. Secondly, NO<sub>2</sub> DSCDs at the same time resolution  
3 are interpolated on 100 m bins as obtained from the first calculation step. Thirdly, absolute  
4 differences of NO<sub>2</sub> DSCDs are derived for each pair of consecutive interpolated values within 5  
5 km. In a final step, absolute differences are averaged along the car track in order to compute a mean  
6 horizontal gradient for each single car lap.

7

### 8 **3.2.2 Stratospheric NO<sub>2</sub> columns**

9 The stratospheric correction in our study is based on stratospheric NO<sub>2</sub> fields as simulated by the  
10 Bremen 3d CTM (B3dCTM) and scaled to satellite observations from the Global Monitoring  
11 Instrument 2 (GOME-2) over a selected region in the Pacific (180°-140° W, 48°-48.5° N). This  
12 scaling is necessary as there is an offset between modeled and measured NO<sub>2</sub> amounts.

13 Briefly, the B3dCTM, which evolved from SLIMCAT (Chipperfield, 1999), is a combined model  
14 approach based on the “Bremen transport model” (Sinnhuber et al., 2003a) and the chemistry code  
15 of the “Bremen two-dimensional model of the stratosphere and mesosphere” (Sinnhuber et al.,  
16 2003b; Winkler et al., 2008). It is driven by ECMWF ERA Interim meteorological reanalysis fields  
17 (Dee et al., 2011).

18 Exemplary simulated stratospheric NO<sub>2</sub> columns above Vienna as obtained from B3dCTM are  
19 shown in Fig. 5 for 19 October 2015. While stratospheric NO<sub>2</sub> amounts sharply decrease in the  
20 morning due to photolysis of NO<sub>2</sub>, the observed increase of NO<sub>2</sub> over the day is the result of  
21 dinitrogen pentoxide (N<sub>2</sub>O<sub>5</sub>) photolysis. The green rectangle indicates the start (06:57 UT) and end  
22 time (09:56 UT) of car DOAS zenith-sky measurements performed on 19 October 2015 (see also  
23 Table 23).

24

25 3.2.3 In our study, the stratospheric model is only used for the diurnal cycle of the stratospheric  
26 NO<sub>2</sub> column as the absolute value is scaled to GOME-2 satellite observations at the time of  
27 overpass. The uncertainty of the diurnal variation is large at twilight but small during the day as

1 changes in stratospheric NO<sub>2</sub> are small when compared to tropospheric NO<sub>2</sub> columns in polluted  
2 regions, such as the urban area of Vienna. As a rough estimate, the uncertainty of the stratospheric  
3 correction is assumed to be less than 10% or typically  $1 \times 10^{15}$  molec cm<sup>-2</sup>.

### 4

### 5 **3.2.3 Simulation of tropospheric air mass factors**

6 In order to apply appropriate tropospheric air mass factors for the conversion of DSCD<sub>meas</sub> into  
7 VCD<sub>tropo</sub> (see Eq. 1) in our case study, different scenarios were simulated with the radiative transfer  
8 model SCIATRAN (Rozanov et al., 2014). The settings for these scenarios (see Table 4) are based  
9 on typical conditions over the urban area of Vienna during the time when car DOAS zenith-sky  
10 measurements were performed.

11 As a first step, extreme cases in terms of aerosol optical depth (AOD), single scattering albedo  
12 (SSA), and mixing-height (MH) were simulated. The results of the RTM calculations are shown in  
13 Fig. 6, where scenario-based Box-AMFs for an altitude range of up to 3 km are plotted for different  
14 SZAs. The results show that aerosols decrease the Box-AMF for small SZAs (30°). With increasing  
15 SZA, however, the Box-AMF increases, in particular when approaching SZA = 80° and when  
16 aerosol loads are high. Within the aerosol layer, which is assumed to be well-mixed within the  
17 selected MH, the Box-AMF rises linearly with altitude. The results further suggest that SSA has  
18 only a small effect within the selected range of settings. Overall, the results of Fig. 6 suggest that  
19 aerosols strongly affect Box-AMFs as a function of SZA.

20 Based on these results, we have decided to select an AMF used for the conversion of DSCD<sub>meas</sub>  
21 into VCD<sub>tropo</sub> based on an intermediate scenario (AOD = 0.25, SSA = 0.95, and MH = 650 m),  
22 which according to our sensitivity study provides a good compromise. From the sensitivity study  
23 of AMF changes we conclude that all other scenarios are well within 20% of these values selected  
24 for the intermediate scenario (see Fig. 7).

### 25

### 26 **3.2.4 Conversion to tropospheric NO<sub>2</sub> vertical column densities**

1 The conversion of NO<sub>2</sub> DSCDs obtained from car DOAS zenith-sky measurements into NO<sub>2</sub>  
 2 tropospheric vertical column densities (VCD<sub>tropo</sub>) is based on the approach by Wagner et al. (2010)  
 3 and Constantin et al. (2013). The authors of the latter study have used a similar zenith-sky DOAS  
 4 system on a car to derive tropospheric NO<sub>2</sub> amounts in Romania. VCD<sub>tropo</sub> from car DOAS zenith-  
 5 sky measurements is determined via the following equation:

$$6 \quad VCD_{tropo} = \frac{DSCD_{meas} + SCD_{ref} - VCD_{strato} * AMF_{strato}}{AMF_{tropo}}, \quad (1)$$

7 where DSCD<sub>meas</sub> is obtained from the car DOAS zenith-sky measurements by applying the DOAS  
 8 analysis (see Sect. 3.1). SCD<sub>ref</sub> is the slant column in the reference spectrum, which cannot be  
 9 measured directly when applying the zenith-sky viewing mode only. Moreover, SCD<sub>ref</sub> has both  
 10 stratospheric and tropospheric amounts, which are estimated with different approaches in the  
 11 literature: (e.g. Wagner et al., 2010; Constantin et al., 2013; Tack et al., 2015). The residual  
 12 amounts in SCD<sub>ref</sub> (e.g. tropospheric NO<sub>2</sub> signal in SCD<sub>ref</sub> amounts that remain after the subtraction  
 13 of stratospheric NO<sub>2</sub> amounts, see Eq. 1) in our study is are calculated by applying the an empirical  
 14 relationship between VCD<sub>tropo</sub> and in situ NO<sub>2</sub> mixing ratios as reported in Kramer et al. (2008).  
 15 To be more specific, the estimation of tropospheric NO<sub>2</sub> residual amounts in SCD<sub>ref</sub> is conducted  
 16 for the time and location of the three selected reference measurements taken in rural areas outside  
 17 the boundaries of Vienna and about 13 km (10 April 2015, 10:49 UT, SZA = 49.8°, 48° 17' 52.08''  
 18 N & 16° 33' 44.64'' E) and 3 km (27 September, 10:17 UT, SZA = 50.33°, 48° 21' 52.75'' N &  
 19 16° 31' 20.24'' E and 23 October, 10:14 UT, SZA = 59.96°, 48° 21' 53.85'' N & 16° 31' 22.48''  
 20 E) away from the nearest air quality monitoring station. More details on data from air quality  
 21 monitoring stations are given in the following Sect. 3.3. Stratospheric vertical column densities  
 22 (VCD<sub>strato</sub> ~~is~~ are) are derived from B3dCTM simulations and scaled to GOME-2 observations (see Sect.  
 23 3.2.2). Stratospheric and tropospheric air mass air mass factors (AMF<sub>strato</sub>) are calculated with the  
 24 SCIATRAN radiative transfer model (Rozanov et al., 2014). For the latter case, the AMF is  
 25 calculated for a wavelength of 460 nm by assuming that NO<sub>2</sub> is well-mixed between the ground  
 26 surface and an altitude of 1 km. The computed stratospheric and tropospheric AMFs) and shown  
 27 in Fig. 8 as a function of SZA are shown in the left and right panels of Fig. 6, respectively. The  
 28 simulation of tropospheric air mass factors (AMF<sub>tropo</sub>) is described in detail in Sect. 3.2.3.

1 Uncertainties in  $VCD_{\text{tropo}}$  are introduced by uncertainties in the quantities used in Eq. 1. Assuming  
2 that the stratospheric AMF is well known, the uncertainties of  $DSCD_{\text{meas}}$ ,  $SCD_{\text{ref}}$ ,  $SCD_{\text{strato}}$  and  
3  $AMF_{\text{tropo}}$  need to be considered. For a typical situation, an overall uncertainty of 25% is found,  
4 dominated by the assumed 20% uncertainty of the AMF (see Sect. 3.2.3). For situations  
5 approaching twilight, the absolute uncertainty of the stratospheric correction increases, and the  
6 relative uncertainty of the slant column can become the dominating error source. If the background  
7 measurement  $SCD_{\text{ref}}$  cannot be taken in a clean region, then the absolute uncertainty on this  
8 quantity can become large and important for the overall uncertainty (see Wagner et al., 2010). As  
9 our car DOAS zenith-sky measurements were performed after morning twilight and because  $SCD_{\text{ref}}$   
10 was taken outside the city of Vienna in rural areas, an overall uncertainty of 25% seems to be  
11 realistic for our study.

### 13 **3.3 In situ measurements of $\text{NO}_2$**

14 For the estimation of ~~tropospheric  $\text{NO}_2$  residual~~ amounts in  $SCD_{\text{ref}}$  as well as for the comparison of  
15  $\text{NO}_2$   $VCD_{\text{tropo}}$  obtained from car DOAS zenith-sky (see Sect. 4.4) and  $\text{NO}_2$  mixing ratios from  
16 ~~tower DOAS off-axis~~ measurements (see Sect. 4.5) with in situ  $\text{NO}_2$  concentrations, data from  
17 ~~more than a dozen~~<sup>23</sup> air quality monitoring stations in and around Vienna, provided by the  
18 Environment Agency Austria, UBA (Umweltbundesamt), are used. (see Fig. 1). For the detection  
19 of  $\text{NO}_2$  concentrations, Horiba APNA-370 and API M200E ( $\text{NO}_x$ ) instruments are currently used  
20 at most of these stations. In addition, TEI 42i and Horiba APNA-360E instruments are operated at  
21 individual stations (Spangl, 2017). The combined measurement uncertainty for these instruments  
22 is about 10% (W. Spangl, personal communication, 2018).

23 ~~Tropospheric  $\text{NO}_2$  Residual~~ amounts in  $SCD_{\text{ref}}$  are calculated by converting simultaneous in situ  
24  $\text{NO}_2$  measurements from the air quality monitoring stations in Gänserndorf (10 April 2015) and  
25 Wolkersdorf (27 September and 23 October 2015) into  $VCD_{\text{tropo}}$  applying the empirical  
26 relationship between concurrent MAX-DOAS and urban background in situ measurements  
27 (Kramer et al., 2008):

$$28 \quad y = 0.036x + 0.018, \tag{2}$$

1 where  $y$  is the tropospheric  $\text{NO}_2$  VCD (~~tropospheric  $\text{NO}_2$  amount~~residual amounts in  $\text{SCD}_{\text{ref}}$  in our  
2 study) in units of  $10^{16}$  molec  $\text{cm}^{-2}$  and  $x$  denotes the in situ  $\text{NO}_2$  mixing ratios in units ppb. The  
3 conversion of in situ  $\text{NO}_2$  concentrations [ $\mu\text{g m}^{-3}$ ] into in situ  $\text{NO}_2$  mixing ratios [ppb] in our study  
4 is described in Sect. 3.5.

5 ~~The tropospheric background values~~The residual amounts in  $\text{SCD}_{\text{ref}}$  as determined with Eq. 2 are  
6 estimated at  $1.3 \times 10^{15}$ ,  $1.1 \times 10^{15}$ , and  $2.2 \times 10^{15}$  molecules  $\text{cm}^{-2}$  on 10 April, 27 September, and  
7 23 October, respectively. We note that the extrapolation of the empirical relationship to our  
8 measurements is critical in a sense that meteorological conditions and emissions are not the same  
9 in Leicester and Vienna. Due to the fact that  $\text{SCD}_{\text{ref}}$  measurements were taken outside of Vienna in  
10 our study, with in situ measurements of  $\text{NO}_2$  being in the range of 2.5 to 6 ppb on those three days  
11 and indicating rather low ~~tropospheric  $\text{NO}_2$  residual~~ amounts, the error is assumed to be likewise  
12 low in this case.

13 For the comparison of car DOAS zenith-sky and in situ  $\text{NO}_2$  observations, we have selected half-  
14 hour averages of  $\text{NO}_2$  concentrations from seven stations in Lower Austria and eight stations in  
15 Vienna that are within 5 km from the car route (see ~~Table 3~~Fig. 1). The selection of appropriate  
16 in situ  $\text{NO}_2$  observations for the comparison with tower DOAS off-axis measurements is described  
17 in Sect. 4.5. For both cases, half-hour averages of  $\text{NO}_2$  concentrations are converted into mixing  
18 ratios (see Sect. 3.5).

### 20 **3.4 Mixing-height from ceilometer observations**

21 The conversion of  $\text{VCD}_{\text{tropo}}$  into mixing ratios as described in the following Sect. 3.5 requires,  
22 besides meteorological measurements of pressure and temperature, information on the planetary  
23 boundary layer depth (also known as mixing-height). The Austrian official weather service, ZAMG  
24 (Zentralanstalt für Meteorologie und Geodynamik), performs operational aerosol-layer height  
25 measurements with a Vaisala CL51 ceilometer at the Hohe Warte site in the North West of Vienna  
26 ( $48^\circ 14' 55''$  N,  $16^\circ 21' 23''$  E). Mixing-height (MH) time series are obtained from these  
27 measurements by removing unrealistic nocturnal aerosol-layer height values, avoiding outliers,  
28 filling data gaps by linear interpolation, and smoothing (Lotteraner and Piringer, 2016). Mixing-

1 height data at a temporal resolution of 5 minutes were provided by ZAMG for those days when car  
2 DOAS zenith-sky measurements were carried out.

### 3 4 **3.5 Comparison of NO<sub>2</sub> mixing ratios obtained from car DOAS zenith-sky and in situ** 5 **measurements**

6 The comparison between the two independent NO<sub>2</sub> observations (car DOAS zenith-sky versus in  
7 situ) is based on gridding the data of both measurement techniques onto a 0.01° x 0.01° spatial  
8 resolution. For a better comparison, NO<sub>2</sub> VCD<sub>tropo</sub> as obtained from car DOAS zenith-sky  
9 measurements as well as in situ NO<sub>2</sub> concentrations are converted into mixing ratios. The former  
10 conversion is based on recommendations made in Knepp et al. (2013). The authors of that study  
11 have converted Pandora tropospheric NO<sub>2</sub> values into mixing ratio values by applying a planetary  
12 boundary layer (PBL) height correction factor. Although this approach assumes a constant mixing  
13 ratio in the PBL, which is not necessarily correct in an urban environment, it accounts for the  
14 variability in MH throughout the day. We follow their approach and estimate boundary layer  
15 mixing ratios of NO<sub>2</sub> (X<sub>NO<sub>2</sub></sub>) via the following equation:

$$16 \text{ Car DOAS (BL) } X_{NO_2} = \frac{VCD_{tropo}}{MH * n_a}, \quad (3)$$

17 where MH is the mixing-height (PBL in their study) and n<sub>a</sub> denotes the number density of air (N  
18 in their study). Here, we use lap averages for MH as calculated from the data in 5 minute resolution  
19 provided by ZAMG (see Sect. 3.4). The standard deviation of these lap averages generally ranges  
20 between 10 and 50 m but can be as high as 200 m when wind speeds are high (see Table 23). The  
21 number density of air, which is related to the atmospheric pressure by the ideal gas law, is also  
22 averaged over the individual car laps. Meteorological measurements of pressure (p) and  
23 temperature (T) used for the calculation of n<sub>a</sub> are provided by the BOKU (Universität für  
24 Bodenkultur) weather station, located in the North-Westnorthwest of Vienna (48° 14' 16.45" N,  
25 16° 19' 54" E). We note that the weather station is located about 100 m higher than the altitude  
26 level of the car route. Thus, pressure might be slightly lower when compared to the pressure level  
27 100 m below. On the other hand, the weather station is also located outside of the city center, at  
28 the foot of the hills in the Northwest and in a less densely populated residential area with many



1 green areas, resulting in slightly cooler temperatures than expected for other places along the car  
2 route. Following this reasoning, it becomes clear that the altitude difference might cancel in the  
3 calculation of  $n_a$  (see Eq. 3) and also in the following Eq. 5.

4 Recently, Dieudonne et al. (2013) highlighted the fact that large vertical gradients of  $\text{NO}_2$   
5 concentrations exist over urban areas. The authors of that study suggest that the averaged  
6 concentration within the PBL is only about 25% of  $\text{NO}_2$  surface concentration measurements when  
7  $\text{NO}_2$  profiles from chemistry-transport models are assumed for the PBL. Following this reasoning,  
8 Car DOAS (BL)  $X_{\text{NO}_2}$  as estimated via Eq. 3 does not represent  $\text{NO}_2$  near-surface mixing ratios  
9 sufficiently well and a comparison with  $\text{NO}_2$  as obtained from air quality monitoring stations and  
10 converted into In situ  $X_{\text{NO}_2}$  (see Eq. 5) is not yet reasonable. Consequently, an empirical approach  
11 for estimating near-surface  $\text{NO}_2$  mixing ratios from the car DOAS zenith-sky measurements ~~was~~  
12 ~~developed~~ *is introduced in our study*, in addition to Car DOAS (BL)  $X_{\text{NO}_2}$ .

13 In order to achieve optimal agreement between car DOAS zenith-sky measurements and in situ  
14 observations in our study, we include four parameters that are expected to affect the vertical  $\text{NO}_2$   
15 gradients and conduct a linear regression analysis as follows:

$$16 \quad Y = \beta_0 + \beta_1 X_1 + \beta_2 X_2 + \beta_3 X_3 + \beta_4 X_4 + \varepsilon, \quad (4)$$

17 where  $Y$  is the expected value of the dependent variable In situ  $X_{\text{NO}_2}$  (see Eq. 5) and  $X_1$ ,  $X_2$ ,  $X_3$ ,  
18 and  $X_4$  are the independent variables  $\text{VCD}_{\text{tropo}} \text{NO}_2$ , MH, wind speed, and  $n_a$ , respectively (see  
19 Table 23).

20 The conversion of in situ  $\text{NO}_2$  concentrations ( $c_m$ ) into mixing ratios is based on the equation:

$$21 \quad \text{In situ } X_{\text{NO}_2} = c_m \frac{1}{M_i} * \frac{RT}{p}, \quad (5)$$

22 where  $M_i$  is the molecular weight of  $\text{NO}_2$  and  $R$  denotes the universal gas constant. As for the  
23 calculation of  $n_a$ ,  $p$  and  $T$  measurements at a 10 minute resolution are taken from the BOKU  
24 weather station and averaged for the individual car laps.

25 All  $\text{NO}_2$  mixing ratio values within individual grid cells are averaged and then compared with each  
26 other.

1

## 2 **3.6 Meteorological measurements of wind direction and wind speed**

3 Most of the emission sources other than traffic are located in the South-East of Vienna. The wind  
4 blew exactly from this direction on several days when car DOAS zenith-sky measurements were  
5 carried out. In addition, the car journey was planned to include the motorway along the Danube  
6 River, spanning a distance of about 20 km from North-West ( $48^{\circ} 21' 25''$  N,  $16^{\circ} 18' 25''$  E) to  
7 South-East ( $48^{\circ} 12' 32''$  N,  $16^{\circ} 26' 24''$  E). These are prerequisites for the optimal analysis of the  
8 evolution of  $\text{NO}_2$  in space and time, in particular on days where wind was blowing either from  
9 North-West (NW) or South-East (SE). As there are no large sources of  $\text{NO}_x$  located in the NW, we  
10 rather focus on days when wind was blowing from the SE.

11 Data on wind direction and wind speed are provided by ZAMG. We have selected such data from  
12 four stations in Lower Austria and five stations in Vienna that are in close proximity to the car  
13 route (see Table 45). The temporal resolution of these measurements is 10 minutes. Instead of  
14 attempting to map the wind direction to the car route in time, we have averaged these measurements  
15 over the period between start and end time of each car journey and calculated the standard deviation  
16 (see Table 23).

17

## 18 **3.7 Tower DOAS measurements of tropospheric $\text{NO}_2$**

### 19 **3.7.1 Temporal resolution and normalization of $\text{NO}_2$ DSCDs with $\text{O}_4$**

20 Compared to the car DOAS zenith-sky measurements, the temporal resolution of spectral  
21 measurements performed on the rotating tower platform is higher (0.025 s). This is because of the  
22 relatively fast rotation speed resulting in a full  $360^{\circ}$  rotation within only 26.5 minutes. Again, these  
23 temporally high-resolved spectral measurements are averaged, but this time over 10 seconds. After  
24 the averaging procedure, roughly 150 measurements remain for a single  $360^{\circ}$  rotation. These  
25 observations are then interpolated on  $3.6^{\circ}$  segments, resulting in 100 measurements for one single  
26 rotation.

1 One of the main drawbacks of the measurements is that only one reference measurement was taken  
2 after the measurements. This was because no zenith-sky measurement was possible from within  
3 the restaurant, and no second DOAS system was available during that time for parallel  
4 measurements from the surface. Therefore, a fixed zenith spectrum has to be used instead of a  
5 sequential one, resulting in an increasing effect of a changing tropospheric light path (e.g. due to  
6 geometry, aerosols, phase function etc.) with increasing time difference between the off-axis and  
7 fixed zenith spectra. One way of overcoming this problem is to normalize NO<sub>2</sub> DSCDs with O<sub>4</sub>  
8 DSCDs, which is done for all measurements taken.

9

### 10 3.7.2 Computation of path-averaged NO<sub>2</sub> mixing ratios

11 A modified geometrical approach (MGA) for estimating long-path averaged mixing ratios of trace  
12 gases (e.g. NO<sub>2</sub>) from MAX-DOAS measurements at high-altitude sites was proposed in a recent  
13 study by Gomez et al. (2014). The method assumes a single-scattering geometry and a scattering  
14 point altitude close to that of the instrument. Under these assumptions, the slant paths of the  
15 zenith ( $\alpha = 90^\circ$ ) and horizontal ( $\alpha = 0^\circ$ ) measurements are identical up to the scattering point  
16 and thus, cancel in the DSCD when using a zenith-sky background spectrum close in time. For  
17 measurements performed at higher altitudes, the MGA can be applied without any correction  
18 factors, in particular when the instrument is located well above the PBL and aerosol amounts are  
19 negligibly low (Schreier et al., 2016). For MAX-DOAS measurements carried out close to the  
20 ground level, however, the MGA is limited because of a substantial aerosol load and correction  
21 factors are needed (Sinnreich et al., 2013). Nevertheless, Seyler et al. (2017) have recently  
22 successfully utilized the MGA for MAX-DOAS measurements of shipping emissions in the  
23 German Bight – without the use of correction factors. According to their findings, typical lengths  
24 of horizontal light paths in the visible spectral range are in the range of 12.9±4.5 km on average  
25 and can reach up to 15 km on days with optimal visibility. It should be noted, however, that the  
26 non-consideration of correction factors in polluted environments such as the German Bight will  
27 lead to a systematic overestimation of horizontal path lengths, depending on the aerosol load.

28 In our study, where the rotating tower platform is also located close to the ground level, we  
29 overcome this problem by making the following assumptions. Firstly, we assume that the signal

1 for horizontal measurements ( $\alpha = 0^\circ$ ) is dominated by the horizontal part of the light path after the  
2 last scattering event. Secondly, a hill named Kahlenberg (484 m a.s.l.) and being located in the  
3 Northwest of the Vienna Danube Tower ( $305^\circ$ ) comes into field of view once every rotation. We  
4 assume that the hill limits the horizontal optical path length (hOPL) under clear sky conditions and  
5 use the distance between the summit of the hill and the Vienna Danube Tower (6.95 km) as  
6 normalization value. The conversion of DSCD  $O_4$  at  $\alpha = 0^\circ$  is realized by relating this distance with  
7 the obtained DSCD  $O_4$  value at  $305^\circ$  and applying the resulting relationship to all other DSCD  $O_4$   
8 values observed during the same tower platform rotation. We assume that the change of DSCD  
9  $NO_2$  in the vertical ( $\alpha = 90^\circ$ ) can be neglected for (polluted) urban environments over the course  
10 of one tower rotation. The latter assumption has to be made because no sequential zenith-sky  
11 spectra are available. Therefore, path-averaged  $NO_2$  mixing ratios are only estimated and presented  
12 for the last tower rotations of the individual days, having the zenith-sky reference spectrum as close  
13 as possible in time.

14 When taking all these assumptions into consideration, path-averaged mixing ratios of  $NO_2$  can be  
15 estimated with the following equation:

$$16 \quad \text{Tower DOAS } X_{NO_2} = \left( \frac{DSCD \text{ } NO_2}{hOPL} \right) / n_a \quad (6)$$

17 For the calculation of  $n_a$ , rotation averages of pressure and temperature as provided by the BOKU  
18 weather station are used (see Sect. 3.5).

19

## 20 **4 Results and discussion**

### 21 **4.1 Horizontal gradients of $NO_2$ DSCDs**

22 As the car DOAS zenith-sky measurements provide in addition to the temporal distribution the  
23 horizontal variation of  $NO_2$ , the method described in Sect. 3.2.1 is applied to the car DOAS zenith-  
24 sky observations to determine horizontal gradients of  $NO_2$ .

25 In Figure 79, typical examples of such horizontal gradients are presented for 27 September, 6  
26 October and 3 November 2015 – three days with different wind conditions, temperature levels and

1 tropospheric NO<sub>2</sub> amounts (see Table 23). In general, an increase in absolute NO<sub>2</sub> differences with  
2 increasing distance from the individual starting points is found. While absolute NO<sub>2</sub> differences  
3 sharply increase within the first one or two kilometers for most of the journeys, the increase  
4 significantly weakens during the remaining kilometers. During the first kilometer, absolute NO<sub>2</sub>  
5 differences increase by a factor of 1.5 to 4, depending on the overall NO<sub>2</sub> level on the investigated  
6 days. While the absolute NO<sub>2</sub> differences rise by a factor of about two within the first two  
7 kilometers on 27 September, an increase by a factor of almost four is found for the same distance  
8 on the more polluted 6 October 2015.

9 The results imply that the magnitude of absolute NO<sub>2</sub> differences is linked to the magnitude of  
10 tropospheric NO<sub>2</sub> amounts observed. On the other hand, it is difficult to detect the factors affecting  
11 the shape of the derived curves. Interestingly, we found only small differences in the shape and  
12 magnitude of horizontal NO<sub>2</sub> gradients when comparing individual car journeys of single days with  
13 each other. Only for days with significant changes in wind direction (e.g. 27 September 2015) ~~are~~  
14 the differences in magnitude are obvious, when the single laps are compared with each other. While  
15 the curves of 10 April (not shown) and 6 October are similar in shape, the typical sharp increase  
16 within the first two kilometers is not observed for 3 November, although average values of wind  
17 speed, wind direction and mixing-height were similar on those days (see Table 23). It is not clear  
18 why the shape of NO<sub>2</sub> as a function of distance observed on 3 November differs from those found  
19 on the other two days. One reason could be variations in photochemistry and/or emissions and/or  
20 dilution of NO<sub>x</sub>. It is interesting to note that 3 November 2015 was clearly the coldest day with  
21 temperatures below 5°C (see Table 23). As a result, we argue that the characteristic horizontal NO<sub>2</sub>  
22 scale of the observed NO<sub>2</sub> fields in Vienna is on the order of 1 to 2 km.

23

#### 24 **4.2 Temporal evolution** **Spatio-temporal patterns** of tropospheric NO<sub>2</sub> **obtained from** 25 **car DOAS zenith-sky measurements**

26 Figure 810 shows typical car DOAS zenith-sky measurements of NO<sub>2</sub> performed on 10 April 2015.  
27 The black and red curves represent DSCD<sub>meas</sub> and VCD<sub>tropo</sub>, respectively. The stratospheric NO<sub>2</sub>  
28 amounts as simulated by B3dCTM and scaled to GOME-2 observations (see Sect. 3.2.32) are  
29 illustrated by the blue line. Clearly, stratospheric NO<sub>2</sub> is relatively low in this case of increased

1 tropospheric NO<sub>2</sub> levels when compared to VCD<sub>tropo</sub>. The relatively small diurnal increase of NO<sub>2</sub>  
2 in the stratosphere can hardly be seen for the 6-hour period. There are individual peaks in NO<sub>2</sub>  
3 throughout the morning of 10 April 2015. While the longer lasting NO<sub>2</sub> peaks are probably  
4 connected to pollution from traffic, sharp peaks rather indicate some outflow of NO<sub>2</sub> from the  
5 refinery and/or other local static emission sources. The magnitude of observed NO<sub>2</sub> VCD<sub>tropo</sub> is in  
6 good agreement with measurements performed around the German cities Mannheim and  
7 Ludwigshafen as well as in the Romanian city Braila (Ibrahim et al., 2010; Dragomir et al., 2015).  
8 As expected, significantly higher values of NO<sub>2</sub> VCD<sub>tropo</sub> were observed by Wang et al. (2012) in  
9 the central urban area of Shanghai, China.

10 In the following, the small-scale transport of NO<sub>2</sub> is evaluated along the Donauufer motorway  
11 (A22) in more detail. The A22 motorway, which is identifiable in Fig. 1 by azure blue and turquoise  
12 dots (NW to SE), is one of the busiest roads in Vienna, in particular in the south-eastern area, where  
13 many commuters take the Südosttangente motorway (A23) at the motorway junction  
14 Kaisermühlen. The A23 is another busy road in Austria having about 160000 passenger cars  
15 driving every day on average (www.vcoe.at). As a consequence, NO<sub>2</sub> levels are expected to be  
16 significantly increased in this area, in particular during the morning and evening rush hours.

17 The NO<sub>2</sub> variation along the A22 motorway is shown in Fig. 911 for Friday, 10 April and Friday,  
18 3 November 2015 as a function of cumulative distance, where the starting and end points are in the  
19 NW and SE of the A22 motorway. The red, blue, and green curves represent NO<sub>2</sub> VCD<sub>tropo</sub> during  
20 the first, second, and third drive, respectively. In order to not confuse the reader, the first and second  
21 rounds of days with measurements taken only during two rounds are here referred to as round two  
22 and three, starting approximately at 07:00 and 08:30 UT, respectively (see Table 23). While wind  
23 was blowing from SE on both days, averages of wind speed were slightly higher on 3 November.

24 On 10 April, highest NO<sub>2</sub> VCD<sub>tropo</sub> is observed in the SE rather than in the NW during the first  
25 drive. This seems reasonable as the traffic volume is generally largest in this area, in particular  
26 during the morning rush-hour, which is captured by the first drive of that day. NO<sub>2</sub> loads are then  
27 moving to the NW of the A22 motorway, because air masses are transported from SE. A clear shift  
28 of NO<sub>2</sub> pollution from SE to NW is observed on 10 April 2015. Highest NO<sub>2</sub> VCD<sub>tropo</sub> during the  
29 first ( $\sim 2.3 (>1.5) \times 10^{16}$  molec cm<sup>-2</sup>), second ( $< 2.50 \times 10^{16}$  molec cm<sup>-2</sup>), and third drive ( $> 2.5 \times 10^{16}$

1 molec cm<sup>-2</sup>) are located around 19.5, 18.5, and 8.5 km away from the starting point in the NW,  
2 respectively. Interestingly, the observed NO<sub>2</sub> peak during the last drive is very pronounced. We  
3 attribute this to the NO<sub>2</sub> formation via the chemical reaction of NO with ozone towards noon time.  
4 The topography in this area could also be responsible for these high NO<sub>2</sub> levels. There are two hills  
5 left (Bisamberg, 358 m a.s.l.) and right (Kahlenberg, 484 m a.s.l.) of the Danube River. As a  
6 consequence, the pollution load could be channeled between the two hills, leading to a localized  
7 increase in NO<sub>2</sub> amounts in this area.

8 The distance of NO<sub>2</sub> transport appears larger between the second and third drives when compared  
9 with distances of NO<sub>2</sub> transport between the first and second journey. This might be related to the  
10 increase in average wind speed throughout the morning (see Table 23). Overall, the distance of  
11 NO<sub>2</sub> transport on 10 April 2015 is in good agreement with average wind speed. Due to higher wind  
12 speeds on 3 November 2015, the expected peaks of NO<sub>2</sub> in the NW during the third journey cannot  
13 be seen anymore. This might be related to the high averaged wind speeds during the second and  
14 third drives (between 8 and 10 km h<sup>-1</sup>) and thus, a distance of transport exceeding the area of  
15 evaluation. On the other hand, a clear shift of elevated NO<sub>2</sub> amounts into the NW is also observed  
16 for the second round on 3 November 2015. It is interesting to note that the horizontal extent of  
17 elevated NO<sub>2</sub> amounts during the third round of 10 April and during the second round of 3  
18 November 2015 spans about 8 km in both cases – under similar wind speeds. We argue that this is  
19 a characteristic horizontal extent of a NO<sub>2</sub> plume resulting from morning rush-hour traffic in  
20 Vienna under calm southeasterly winds.

### 21 22 **4.3 Spatio-temporal patterns of tropospheric NO<sub>2</sub> obtained from tower DOAS off-** 23 **axis measurements**

24 The spatial and temporal variation in tropospheric NO<sub>2</sub> amounts is also evaluated by analyzing the  
25 tower DOAS off-axis measurements. In order to correct light path lengths in the troposphere, NO<sub>2</sub>  
26 DSCDs are normalized with O<sub>4</sub> DSCDs. When looking at the time series of intensity (see Fig. 2),  
27 NO<sub>2</sub>, and O<sub>4</sub> (Fig. 4012), it becomes apparent that these parameters show variations as a function  
28 of azimuth angle. This variation is repeated with each further tower platform rotation. Although  
29 some similarity is found between DSCD NO<sub>2</sub> and O<sub>4</sub>, the highest and lowest amounts of both trace

1 gases are somehow shifted on the x-axis. Some similarity between DSCD  $O_4$  and  $NO_2$ , which is  
2 observed on all five days (not shown), is attributed to changes in the light path. Interestingly, the  
3 normalization with  $O_4$  slightly changes the azimuthal position of the pollution peaks towards the  
4 city center.

5 The geographical distribution of DSCD  $NO_2/O_4$  is shown in Fig. 413 for 10 May 2016, when  
6 tower DOAS off-axis measurements during nine platform rotations were collected. The values  
7 plotted on the map are mean  $NO_2/O_4$  values and the radius is the  $O_4$  column. On that day, wind was  
8 mainly blowing from easterly to southeasterly directions. As a result, highest  $NO_2/O_4$  ratios are  
9 observed towards the city center.

10 The spatial and temporal variability of DSCD  $NO_2/O_4$  as obtained from tower DOAS off-axis  
11 measurements is shown in Fig. 4214 for 9 and 10 May 2016. As already identified from the analysis  
12 of the car DOAS zenith-sky measurements, highest tropospheric  $NO_2$  over Vienna is found in the  
13 early morning – a consequence of both a lower (nocturnal) mixing-height and emissions of  $NO_x$   
14 from morning rush hour traffic. Highest  $NO_2$  amounts on both days are generally observed over  
15 the city center of Vienna, which is located to the Southwest of the Vienna Danube Tower. A closer  
16 look suggests that DSCD  $NO_2/O_4$  is about a factor two larger on 9 May than on the 10 May. While  
17 wind was constantly blowing from the SE on both days, the explanation for this is most likely the  
18 higher wind speeds on 10 May.

#### 19 20 **4.34 Comparison of $NO_2$ from car DOAS zenith-sky measurements with in situ $NO_2$**

21 The spatial and temporal evolution of  $NO_2$  on 10 April 2015 in Vienna as observed by car DOAS  
22 zenith-sky (dots) and in situ measurements (squares) is shown in Fig. 4315. Wind direction and  
23 wind speed obtained from local weather stations are indicated by white arrows. The geographical  
24 maps illustrate the spatial distribution of tropospheric  $NO_2$  during the three performed journeys on  
25 that day. As already highlighted in Sect. 4.2, a clear change in the amount of  $NO_2$  throughout the  
26 morning is observed along the motorway A22. A large proportion of observed  $NO_2$  amounts is  
27 produced from traffic emissions of  $NO_x$  during the morning rush-hour traffic, in particular in the  
28 area southeast of the city center. During the time period of about 4.5 hours between starting and



1 end point of the measurements performed on that day, NO<sub>2</sub> is transported over a distance between  
2 10 and 15 km. Another hotspot of increased NO<sub>2</sub> levels is observed close to an oil refinery in the  
3 SE. The outflow of the refinery is in good agreement with wind direction on that day. As already  
4 mentioned in Sect. 4.2, such peaks of NO<sub>2</sub> amounts as a result of local static emission sources are  
5 sharper than those originating from typical rush-hour traffic. There is a clear decrease of  
6 tropospheric NO<sub>2</sub> throughout the morning (see also Table 23), most likely as a consequence of  
7 dilution and/or the reaction of NO<sub>2</sub> with the hydroxyl radical (OH), which is the largest NO<sub>x</sub> sink  
8 during daytime.

9 Overall, averages of tropospheric NO<sub>2</sub> observations were highest on 10 April 2015 and 3 November  
10 2015. We attribute this behavior to the comparatively low wind speeds, and consequent low  
11 dilution.

12 As outlined in Sect. 3.5, the correlation of the two data sets (car DOAS zenith-sky versus in situ)  
13 uses data converted into NO<sub>2</sub> mixing ratios, which are gridded values onto 0.01° x 0.01° cells. The  
14 correlation is performed for each single day where car DOAS zenith-sky measurements were  
15 carried out. The scatter plots including statistics about slope, intercept and correlation coefficient  
16 are illustrated in Fig. 1416. Each of the diamonds represents a grid box average of X<sub>NO2</sub> from car  
17 DOAS zenith-sky measurements as a function of averaged X<sub>NO2</sub> concentrations from in situ  
18 monitors. The correlation coefficient on 10 April 2015, for example, is 0.8, suggesting a close  
19 linear relationship of the two independent NO<sub>2</sub> measurements on that day (see also Table 23). The  
20 negative offset apparent implies that in situ X<sub>NO2</sub> is higher than X<sub>NO2</sub> estimated via Eq. 3. While  
21 this is the case for the grid box averages calculated from measurements taken during the second  
22 and third journeys of that day, X<sub>NO2</sub> from car DOAS zenith-sky observations seem to be  
23 overestimated during the first journey. X<sub>NO2</sub> values close to the 1:1 line are also observed on 2  
24 October, the second day, when early morning measurements were performed and when wind was  
25 also blowing from Southeast. The reason for the better agreement in the early morning (e.g. during  
26 the first car journey) could be the lower MH and lower wind speed, resulting in a better vertical  
27 mixing within the shallow boundary layer. The increase in both MH and wind speed throughout  
28 the morning might counteract a vertical mixing of NO<sub>2</sub> loads.

1 Another explanation of the rather underestimated mixing ratio values obtained from car DOAS  
2 zenith-sky measurements observed on the other days is a possible overestimation of tropospheric  
3 AMFs, which are used for the conversion of NO<sub>2</sub> DSCDs (see Eq. 1). Wang et al. (2012) have  
4 reported total uncertainties of tropospheric AMFs in the range of 20-30% for SZAs<40°. With  
5 increasing SZA towards sunrise/sunset the uncertainties further increase. We note that most of our  
6 car DOAS zenith-sky measurements were performed for SZAs larger than 40°.

7 Kramer et al. (2008) performed a comparison between data from a Concurrent MAX-DOAS  
8 (CMAX-DOAS) instrument and in situ instruments in the city of Leicester, England. They  
9 highlighted the fact that the relative positions of the in situ instruments to the streets affect the  
10 comparison. In contrast to their study, car DOAS zenith-sky measurements were performed along  
11 motorways in our study. Therefore, this effect can be partly ruled out for the comparison presented  
12 in our study. Difficulties rather arise from losing some of the NO<sub>2</sub> signal at the surface levels  
13 because of the zenith-sky geometry applied for our car DOAS measurements.

14 Nevertheless, large correlation coefficients ( $R = 0.72-0.94$ ) are also observed on the other days  
15 with wind coming from the SE (6, 27 October, and 3 November). In contrast, weak correlation  
16 between the two data sets is observed on days when wind was blowing from the NW (27  
17 September, 19 and 23 October). The reason for the weak correlation on those days is not entirely  
18 clear. However, a closer look reveals that the variability of NO<sub>2</sub> levels between the performed car  
19 journeys on a single day is only low on days with winds from NW (see Table 23). This might be  
20 related to the fact that high traffic volume but also most of the in situ monitoring station used in  
21 this study are located rather in the SE of the city center than in the NW and thus, the peak of rush-  
22 hour traffic does not show up in the measurements of most of the in situ monitoring stations on  
23 those days.

24 As  $X_{NO_2}$  estimated via Eq. 3 represent averages within the PBL and thus, values are rather  
25 underestimated when compared to the values obtained from air quality monitoring stations (see  
26 Table 23), a linear regression analysis is introduced (see Eq. 4). The motivation behind this  
27 approach is related to the findings of Dieudonne et al. (2013). The authors of that study highlighted  
28 the fact that the vertical distribution of NO<sub>2</sub> within the PBL over an urban area is not homogenous.

1 They also suggested considering the effect of wind speed on the vertical gradient. Therefore, we  
2 also include wind speed in the linear regression analysis.

3 The lap averages of Car DOAS (Surface)  $X_{\text{NO}_2}$  are given in Table 23. Overall, the values are in  
4 good agreement with the lap averages obtained from the air quality monitoring stations. For a better  
5 view, the modeled mixing ratios are plotted against mixing ratios obtained from in situ  
6 measurements in Fig. 1517. The gray dotted lines represent the  $\pm 25\%$  level, meaning that all the  
7 values estimated via Eq. 4 are within  $\pm 25\%$ , with the exception of values lower than 10 ppb. The  
8 reason for these larger differences could be a reduced signal-to-noise of the car DOAS zenith-sky  
9 measurements and consequently larger errors in the  $\text{NO}_2$  DSCDs. Nevertheless, the high correlation  
10 coefficient of the linear relationship ( $R = 0.94$ ) is promising, in particular when thinking of  
11 applying this method to  $\text{NO}_2$   $\text{VCD}_{\text{tropo}}$  obtained from long-term MAX-DOAS measurements,  
12 which provide better statistics.

13

#### 14 **4.45 Path-averaged $\text{NO}_2$ mixing ratios obtained from tower DOAS off-axis**

15 Although the  $\text{NO}_2/\text{O}_4$  ratio gives an overall impression of spatiotemporal changes of  $\text{NO}_2$  amounts  
16 over Vienna, an absolute quantification of  $\text{NO}_2$  amounts (e.g. the conversion into mixing ratios) is  
17 not possible with this approach. Therefore, another method is used for the estimation of path-  
18 averaged  $\text{NO}_2$  mixing ratios at 160 m altitude of the rotating tower platform (see Sect. 3.7.2).

19 Estimated horizontal optical path lengths as a function of the azimuthal viewing direction obtained  
20 from measurements taken on 29 April (blue) and 9 May (red) 2016 are shown in Fig. 1618. Both  
21 curves represent the last round measurements recorded during those days, when the reference  
22 zenith-sky measurement was taken shortly afterwards. Overall, higher hOPLs are observed on 9  
23 May, which was a day with wind speeds reaching up to  $15 \text{ km h}^{-1}$ . The exceptionally low wind  
24 speeds observed on 29 April ( $< 5 \text{ km h}^{-1}$ ) explain the lower values of hOPL on that day. Low values  
25 of hOPL are generally linked to low visibility, which is the result of an increased aerosol  
26 accumulation over emission hot spots on that otherwise cloudless day. As aerosols largely affect  
27 hOPL under such conditions (Sinreich et al., 2013), it is reasonable that lowest values (5-6 km) are  
28 preferably found in off-axis directions between Eastern and Southern directions, which include

1 areas with high traffic roads and industry. In contrast, highest hOPLs are observed in the North of  
2 the Vienna Danube Tower on both days (10-11 km). This is reasonable because those regions are  
3 known as rather rural areas without significant emission sources. The highest hOPLs estimated in  
4 our study are slightly lower than the mean value (12.9 km) reported in Seyler et al. (2017), but still  
5 within the standard deviation.

6 Although our assumption made on the limitation of the horizontal light path length towards the hill  
7 might be critical, we argue that the distance of 6.95 km between the Vienna Danube Tower and the  
8 summit of that hill is still lower than  $12.9 \pm 4.5$  km and thus seems to be optimal for this  
9 normalization approach.

10 Estimated path-averaged NO<sub>2</sub> mixing ratios are shown for 29 April (blue) and 9 May (red) 2016 in  
11 Fig. 1719. Again, only the last rotations of those days are presented in the graph. As expected from  
12 the observed wind conditions and estimated hOPLs, path-averaged X<sub>NO<sub>2</sub></sub> is higher on 29 April.  
13 Over rural areas, which are located in the North of the Vienna Danube Tower, values are lowest  
14 (2.5 to 4 ppb) on both days. In contrast, highest values (up to 9 ppb) are again observed towards  
15 SE. We note that path-averaged mixing ratios are only shown for two tower rotations, which took  
16 place shortly before noon – at a time when the peak in NO<sub>2</sub> amounts over the city is past.

17 For a better illustration, X<sub>NO<sub>2</sub></sub> as a function of hOPL obtained from the last rotation of tower DOAS  
18 off-axis measurements and X<sub>NO<sub>2</sub></sub> values calculated from simultaneous in situ measurements are  
19 plotted on a geographical map in Fig. 1820 for 29 April (left) and 9 May 2016 (right). We note that  
20 the NO<sub>2</sub> mixing ratios estimated from tower DOAS off-axis measurements are averages over  
21 several kilometers at 160 m above ground, whereas NO<sub>2</sub> mixing ratios from in situ stations rather  
22 represent point measurements at the surface level. The comparison therefore implies that the  
23 variability of NO<sub>2</sub> as observed at 160 m above ground is much less pronounced than that between  
24 the individual ground stations. Moreover, horizontal gradients in 160 m above ground are small.  
25 As already outlined above, highest NO<sub>2</sub> amounts obtained from both measurements are generally  
26 found over the city center and over high traffic roads in the Southeast of the city center on 29 April,  
27 a day with very low wind speeds ( $< 5 \text{ km h}^{-1}$ ). The picture looks different for 9 May, when wind  
28 was blowing from Southeast and wind speeds reached values of up to  $15 \text{ km h}^{-1}$ . Highest NO<sub>2</sub>

1 amounts from tower DOAS off-axis observations are found in parallel to the wind direction in this  
2 case.

3 For a better quantification,  $X_{\text{NO}_2}$  from tower DOAS off-axis measurements as well as  $X_{\text{NO}_2}$  from  
4 in situ are averaged and compared with each other (Fig. 21). While the mean and standard deviation  
5 are calculated by including all individual measurements of the last tower rotations in the former  
6 case, these parameters are computed by including measurements of  $X_{\text{NO}_2}$  from air quality  
7 monitoring stations that fall within the outer circle of tower DOAS off-axis measurements as  
8 determined by hOPL in the latter case. For both tower DOAS off-axis and in situ measurements,  
9 averaged  $X_{\text{NO}_2}$  are larger by a factor of two on 29 April than on 9 May. On both days, averaged  
10  $\text{NO}_2$  mixing ratios are about a factor ~~four~~ of 6.5 larger at the surface level when compared with  
11 averaged path-averaged values at 160 m above, ~~which. This difference~~ is ~~in good agreement~~  
12 ~~with much larger than~~ the 25% difference reported in Dieudonne et al. (2013), who compared  
13 surface concentrations with in situ concentrations at 300 m above ground in Paris. One reason for  
14 the larger factor found in our study might be an overestimation of mean  $X_{\text{NO}_2}$  at the surface level  
15 due to the relatively large number of air quality monitoring stations close to the city center, where  
16 higher pollution levels are expected. On the other hand, low values of mean  $X_{\text{NO}_2}$  at 160 m above  
17 ground arise from the long light paths, which partly include areas with lower traffic density,  
18 especially in the north of the Danube River. Although a quantification and comparison is  
19 challenging for this case study with only a small amount of data, interesting insights into  $\text{NO}_2$   
20 distributions in the boundary layer above the urban area of Vienna can be gained.

21

## 22 **5 Summary and outlook**

23 In this case study, ~~unique~~ ground-based remote sensing measurements have been coupled with  
24 surface in situ measurements to investigate the  $\text{NO}_2$  distributions in the planetary boundary layer  
25 in the Viennese metropolitan area.

26 A DOAS instrument was used for the determination of the spatial and temporal  $\text{NO}_2$  distributions  
27 in and around the urban area of Vienna. The instrument was applied in two different measurement  
28 setups: Car DOAS zenith-sky and tower DOAS off-axis. The former DOAS-type approach, which

Formatte

1 is already well established and documented in the literature, was used for a total of twenty identical  
2 car journeys, which were carried out on nine days in April, September, October, and November  
3 2015 during the morning hours. The latter configuration is innovative in the sense that horizontal  
4 measurements for more than 100 azimuthal angles are possible within a  $360^\circ$  rotation and within  
5 less than half an hour. The latter setup was used for collecting more than thirty rotations of spectral  
6 measurements on five days in April and May 2016.

7 A DOAS fitting procedure, based on recommendations made for the CINDI-2 campaign  
8 ([www.tropomi.eu/data-products/cindi-2](http://www.tropomi.eu/data-products/cindi-2)), is applied to the collected spectral measurements to  
9 retrieve  $\text{NO}_2$  DSCDs. Overall, good fit quality is found for both DOAS-type measurements, in  
10 particular when  $\text{NO}_2$  amounts were high.

11 As the car DOAS zenith-sky measurements include a contribution from both the background and  
12 stratospheric  $\text{NO}_2$ , a correction scheme based on measurements and chemical transport model  
13 simulations is applied. The subsequent conversion of  $\text{NO}_2$  DSCDs into  $\text{NO}_2$   $\text{VCD}_{\text{tropo}}$  is performed  
14 by applying stratospheric and tropospheric AMFs as derived from radiative transfer calculations.

15 In order to correct light path lengths in the troposphere,  $\text{NO}_2$  DSCDs obtained from tower DOAS  
16 off-axis observations are normalized with  $\text{O}_4$  DSCDs in a first step. In a second step, the assumption  
17 that the Kahlenberg (484 m a.s.l) limits the horizontal optical light path length at an azimuth angle  
18 of  $305^\circ$  is made. The distance between the Vienna Danube Tower and the summit of Kahlenberg  
19 (6.95 km) is then used for the normalization of  $\text{O}_4$  DSCDs to obtain horizontal optical path lengths  
20 (hOPLs).

21 By analyzing  $\text{NO}_2$  DSCDs at high temporal resolution along the individual car journeys,  
22 characteristic horizontal  $\text{NO}_2$  changes as a function of distance could be derived. While the absolute  
23 differences between the first and consecutive measurements increases sharply over the first two  
24 kilometers (by a factor of 1.5 to 4), the observed increase clearly weakens during the remaining  
25 kilometers. From this observation we conclude, that 1-2 km is a characteristic scale of the  $\text{NO}_2$   
26 fields observed in Vienna during the morning hours.

27 The analysis of  $\text{NO}_2$   $\text{VCD}_{\text{tropo}}$  from car DOAS zenith-sky and DSCD  $\text{NO}_2/\text{O}_4$  from tower DOAS  
28 off-axis measurements opened up interesting insights into the spatial and temporal variations of

1 NO<sub>2</sub>. The results imply that wind speed and wind direction impact strongly on the NO<sub>2</sub> distributions  
2 in Vienna. By using data on wind speed and wind direction from several stations within the  
3 metropolitan area of Vienna, short-scale NO<sub>2</sub> transport events could be identified.

4 The comparison of VCD<sub>tropo</sub> from car DOAS zenith-sky measurements with in situ NO<sub>2</sub>  
5 concentrations, which is based on the conversion of both quantities into mixing ratios of NO<sub>2</sub> using  
6 existing approaches, revealed good linear correlation for days when the wind was blowing from  
7 the Southeast (R = 0.72-0.94). In contrast, weak correlation was found for days when the wind was  
8 blowing from the Northwest (R < 0.33), which might be related to the relative location of air masses  
9 affected by dense traffic to the selected in situ monitoring stations.

10 Depending on wind conditions, lap averages of near-surface NO<sub>2</sub> mixing ratios (X<sub>NO<sub>2</sub></sub>) estimated  
11 from car DOAS zenith-sky measurements applying a linear regression analysis are in the range of  
12 3.8 to 26.21 ppb and in good agreement with lap averages of X<sub>NO<sub>2</sub></sub> obtained from in situ  
13 measurements. The linear regression analysis, which is introduced for the first time and tested for  
14 the case study-based data in this study, considers wind speed, in addition to mixing-height (MH)  
15 and number density of air n<sub>a</sub>.

16 Taking into account all the assumptions that have been made for the conversion of DSCDs into  
17 VCD<sub>tropo</sub> and also for the subsequent translation of VCD<sub>tropo</sub> into X<sub>NO<sub>2</sub></sub>, the method linear regression  
18 analysis to derive near-surface mixing ratios seems to work well – at least for the lap averages  
19 considered in this study.

20 The estimation of hOPL and X<sub>NO<sub>2</sub></sub> from the tower DOAS off-axis measurements revealed  
21 interesting insights into an upper layer of the PBL, although only few measurements are presented  
22 due to the lack of sequential zenith-sky measurements that could be taken as reference. Overall,  
23 averaged NO<sub>2</sub> mixing ratios are about a factor ~~four~~ 6.5 larger at the surface level when compared  
24 with mean path-averaged values at 160 m above. ~~The path-averaged mixing ratios are about 35%~~  
25 ~~smaller at 160 m above ground, when qualitatively compared to X<sub>NO<sub>2</sub></sub> from car DOAS zenith-sky~~  
26 ~~measurements performed on days with similar wind conditions~~ altitude.

1 Although the NO<sub>2</sub> hourly European maximum dose rate was not exceeded when measurements  
2 were taken, NO<sub>2</sub> amounts in the urban environment of Vienna are substantial, in particular during  
3 morning hours and when wind speeds are low.

4 We note that the idea of performing tower DOAS off-axis measurements was born when car DOAS  
5 zenith-sky measurements were already taken. Due to other priorities and limited manpower at the  
6 time when tower DOAS off-axis measurements were recorded, car DOAS zenith-sky  
7 measurements could not be carried out simultaneously. For future campaigns in Vienna, however,  
8 simultaneous measurements of the two DOAS configurations should be taken into consideration.

9 Future efforts will be made to test the linear regression analysis on measurements from three static  
10 MAX-DOAS instruments, which are located in Vienna as part of the VINDOBONA (Vienna  
11 horizontal and vertical Distribution Observations Of Nitrogen dioxide and Aerosols) project  
12 ([www.doas-vindobona.at](http://www.doas-vindobona.at)). Once the method is mature and optimized, it could also be applied to  
13 satellite measurements of VCD<sub>tropo</sub>. This would help to obtain near-surface mixing ratios of NO<sub>2</sub>  
14 from the integrated column amounts on a global scale.

15 Additional car DOAS zenith-sky and tower DOAS off-axis measurements that complement the  
16 operational performance of the two MAX-DOAS instruments are also foreseen in the future.  
17 Taking these measurements and also data from the relatively large number of air quality monitoring  
18 stations into consideration, Vienna can be seen as an optimal urban location for future satellite  
19 validation campaigns.

20

## 21 **Acknowledgements**

22 This study was funded by the University of Bremen and the Austrian Science Fund (FWF): I 2296-  
23 N29. We like to thank “Amt der Niederösterreichischen Landesregierung“ and “Amt der Wiener  
24 Landesregierung“ for making the air quality data freely available. We wish to acknowledge the  
25 provision of meteorological data by the Austrian official weather service (ZAMG). Christoph  
26 Lotteraner and Martin Piringer (ZAMG) are acknowledged for calculating time-series of mixing-  
27 height at Wien/Hohe Warte. We thank Andreas Hilboll (MARUM-Bremen) for the provision of  
28 simulated stratospheric NO<sub>2</sub> amounts. Last but not least, we want to thank Mario Meyer and the



1 staff from the Vienna Danube Tower for giving us the opportunity to perform experimental  
2 measurements from the rotating Café and for providing technical assistance.

3

4

5

6

7

8

9

10

11

12

13

14

15

16

17

18

19

20

21

1

2

3

4 **References**

5 Anderson, G., Clough, S., Kneizys, F., Chetwynd, J., and Shettle, E.: AFGL atmospheric  
6 constituent profiles (0–120 km), Tech. Rep. AFGL-TR-86-0110, Air Force Geophys. Lab.,  
7 Hanscom Air Force Base, Bedford, Mass., 1986.

8 Chipperfield, M. P.: Multiannual simulations with a three-dimensional chemical transport model,  
9 *J. Geophys. Res.*, 104, 1781–1805, 1999.

10 Constantin, D. E., Merlaud, A., Van Roozendael, M., Voiculescu, M., Fayt, C., Hendrick, F.,  
11 Pinardi, G., and Georgescu, L.: Measurements of tropospheric NO<sub>2</sub> in Romania using a zenith–  
12 sky mobile DOAS system and comparisons with satellite observations, *Sensors*, 13, 3922–3940,  
13 2013.

14 Danckert, T., Fayt, C., Van Roozendael, M., De Smedt, I., Letocart, V., Merlaud, A., and Pinardi,  
15 G.: QDOAS Software, 2015.

16 Dee, D. P., Uppala, S. M., Simmons, A. J., Berrisford, P., Poli, P., Kobayashi, S., Andrae, U.,  
17 Balmaseda, M. A., Balsamo, G., Bauer, P., Bechtold, P., Beljaars, A. C. M., van de Berg, L., Bidlot,  
18 J., Bormann, N., Delsol, C., Dragani, R., Fuentes, M., Geer, A. J., Haimberger, L., Healy, S. B.,  
19 Hersbach, H., Hólm, E. V., Isaksen, L., Kållberg, P., Köhler, M., Matricardi, M., McNally, A. P.,  
20 Monge-Sanz, B. M., Morcrette, J.-J., Park, B.-K., Peubey, C., de Rosnay, P., Tavolato, C., Thépaut,  
21 J.-N., and Vitart, F.: The ERA-Interim reanalysis: configuration and performance of the data  
22 assimilation system, *Q. J. Roy. Meteorol. Soc.*, 137, 553–597, doi:10.1002/qj.828, 2011.

23 Dieudonné, E., Ravetta, F., Pelon, J., Goutail, F., and Pommereau, J.-P.: Linking NO<sub>2</sub> surface  
24 concentration and integrated content in the urban developed atmospheric boundary layer, *Geophys.*  
25 *Res. Lett.*, 40, 1247–1251, doi:10.1002/grl.50242, 2013.

1 Dockery, D. W., Pope, A., Xu, X., Spengler, J. D., Ware, J. H., Fay, M., E., Ferris, B. J., and  
2 Speizer, F. E.: An association between air pollution and mortality in six U.S. cities, New England  
3 Journal of Medicine, 329, 1753-1759, 1993.

4 Dragomir, C. M., Constantin, D.-E., Voiculescu, M., Georgescu, L. P., Merlaud, A., and van  
5 Roozendaal, M.: Modeling results of atmospheric dispersion of NO<sub>2</sub> in an urban area using METI-  
6 LIS and comparison with coincident mobile DOAS measurements, Atmospheric Pollution  
7 Research 6, 503-510, 2015.

8 Fontjin, A., Sabadell, A. J., and Ronco, R. J.: Homogeneous chemiluminescence measurement of  
9 nitric oxide with ozone, Anal. Chem., 42, 575–579, 1970.

10 Frins, E., Bobrowski, N., Osorio, M., Casaballe, N., Belsterli, G., Wagner, T., and Platt, U.:  
11 Scanning and mobile multi-axis DOAS measurements of SO<sub>2</sub> and NO<sub>2</sub> emissions from an electric  
12 power plant in Montevideo, Uruguay, Atmos. Environ. 98, 347-356,  
13 doi:10.1016/j.atmosenv.2014.03.069, 2014.

14 Gomez, L., Navarro-Comas, M., Puentedura, O., Gonzalez, Y., Cuevas, E., and Gil-Ojeda, M.:  
15 Long-path averaged mixing ratios of O<sub>3</sub> and NO<sub>2</sub> in the free troposphere from mountain MAX-  
16 DOAS, Atmos. Meas. Tech., 7, 3373-3386, <https://doi.org/10.5194/amt-7-3373-2014>, 2014.

17 Hermans, C., Vandaele, A., Carleer, M., Fally, S., Colin, R., Jenouvrier, A., Coquart, B., and  
18 Mérienne, M.-F.: Absorption cross-sections of atmospheric constituents: NO<sub>2</sub>, O<sub>2</sub>, and H<sub>2</sub>O,  
19 Environ. Sci. Pollut. Res., 6, 151–158, doi:10.1007/BF02987620, 1999.

20 Heue, K.-P., Richter, A., Bruns, M., Burrows, J. P., v. Friedeburg, C., Platt, U., Pundt, I., Wang, P.,  
21 and Wagner, T.: Validation of SCIAMACHY tropospheric NO<sub>2</sub>-columns with AMAXDOAS  
22 measurements, Atmos. Chem. Phys., 5, 1039–1051, doi:10.5194/acp-5-1039-2005, 2005.

23 Hilboll, A., Richter, A., and Burrows, J. P.: Long-term changes of tropospheric NO<sub>2</sub> over  
24 megacities derived from multiple satellite instruments, Atmos. Chem. Phys., 13, 4145-4169,  
25 doi:10.5194/acp-13-4145-2013, 2013.

1 Hong, Q., Liu, C., Chan, K. L., Hu, Q., Xie, Z., Liu, H., Si, F., and Liu, J.: Ship-based MAX-DOAS  
2 measurements of tropospheric NO<sub>2</sub>, SO<sub>2</sub>, and HCHO distribution along the Yangtze River, *Atmos.*  
3 *Chem. Phys.*, 18, 5931-5951, <https://doi.org/10.5194/acp-18-5931-2018>, 2018.

4 Hönninger, G., von Friedeburg, C., and Platt, U.: Multi axis differential optical absorption  
5 spectroscopy (MAX-DOAS), *Atmos. Chem. Phys.*, 4, 231–254, doi:10.5194/acp-4-231-2004,  
6 2004.

7 Ibrahim, O., Shaiganfar, R., Sinreich, R., Stein, T., Platt, U., and Wagner, T.: Car MAX-DOAS  
8 measurements around entire cities: quantification of NO<sub>x</sub> emissions from the cities of Mannheim  
9 and Ludwigshafen (Germany), *Atmos. Meas. Tech.*, 3, 709-721, doi:10.5194/amt-3-709-2010,  
10 2010.

11 Ionov, D. and Poberovskii, A.: Quantification of NO<sub>x</sub> emission from St Petersburg (Russia) using  
12 mobile DOAS measurements around the entire city, *International Journal of Remote Sensing*, 36:9,  
13 2486-2502, DOI: 10.1080/01431161.2015.1042123, 2015.

14 IPCC: Climate Change 2013: The Physical Science Basis, contribution of Working Group I to the  
15 Fifth Assessment Report of the Intergovernmental Panel on Climate Change, edited by: Stocker,  
16 T. F., Qin, D., Plattner, G.-K., Tignor, M., Allen, S. K., Boschung, J., Nauels, A., Xia, Y., Bex, V.,  
17 and Midgley, P. M., Cambridge Univ. Press, Cambridge, UK and New York, NY, USA, 2013.

18 Johansson, M., Galle, B., Yu, T., Tang, L., Chen, D., Li, H., Li, J. X., and Zhang, Y.: Quantification  
19 20 of total emission of air pollutants from Beijing using mobile mini-DOAS, *Atmos. Environ.* 42,  
20 6926–6933, 2008.

21 Johansson, M., Rivera, C., de Foy, B., Lei, W., Song, J., Zhang, Y., Galle, B., and Molina, L.:  
22 Mobile mini-DOAS measurement of the emission of NO<sub>2</sub> and HCHO from Mexico City, *Atmos.*  
23 *Chem. Phys. Discuss.*, 9, 865–882, 2009.

24 Johansson, M., Rivera, C., de Foy, B., Lei, W., Song, J., Zhang, Y., Galle, B., and Molina,  
25 L.: Mobile mini-DOAS measurement of the emission of NO<sub>2</sub> and HCHO from Mexico City,  
26 *Atmos. Chem. Phys. Discuss.*, 9, 865–882, 2009.

1 Knepp, T., Pippin, M., Crawford, J., Chen, G., Szykman, J., Long, R., Cowen, L., Cede, A.,  
2 Abuhassan, N., Herman, J., Delgado, R., Compton, J., Berkoff, T., Fishman, J., Martins, D.,  
3 Stauffer, R., Thompson, A. M., Weinheimer, A., Knapp, D., Montzka, D., Lenschow, D.,  
4 and Neil, D.: Estimating surface NO<sub>2</sub> and SO<sub>2</sub> mixing ratios from fast-response total column  
5 observations and potential application to geostationary missions, *J. Atmos. Chem.*, D15308,  
6 doi:10.1007/s10874-013-9257-6, 2013.

7 Kramer, L. J., Leigh, R. J., Remedios, J. J., and Monks, P. S.: Comparison of OMI and ground-  
8 based in situ and MAX-DOAS measurements of tropospheric nitrogen dioxide in an urban area, *J.*  
9 *Geophys. Res.*, 113, D16S39, doi:10.1029/2007JD009168, 2008.

10 Künzli, N., Kaiser, R., Medina, S., Studnicka, M., Chanel, O., Filliger, P., Herry, M., Horak Jr, F.,  
11 Puybonnieux-Textier, V., Quénel, P., Schneider, J., Seethaler, R., Vergnaud, J. C., and Sommer,  
12 H.: Public-health impact of outdoor and traffic-related air pollution: A European assessment,  
13 *Lancet*, 356, 795–801, 2000.

14 Kurucz, R. L., Furenchild, I., Brault, J., and Testermann, L.: Solar flux atlas from 296 to 1300 nm,  
15 National Solar Observatory Atlas No. 1, June 1984, 1984.

16 Lee, D. S., Köhler, I., Grobler, E., Rohrer, F., Sausen, R., Gallardo- Klenner, L., Olivier, J. G. J.,  
17 Dentener, F. J., and Bouwman, A. F.: Estimations of global NO(x) emissions and their  
18 uncertainties, *Atmos. Environ.*, 31, 1735–1749, 1997.

19 Lotteraner, C. and Piringer, M.: Mixing-Height Time Series from Operational Ceilometer  
20 Aerosol-Layer Heights, *Bound.-Lay. Meteorol.*, 161, 265–287, [https://doi.org/10.1007/s10546-](https://doi.org/10.1007/s10546-016-0169-2)  
21 [016-0169-2](https://doi.org/10.1007/s10546-016-0169-2), 2016.

22 Meier, A. C., Schönhardt, A., Bösch, T., Richter, A., Seyler, A., Ruhtz, T., Constantin, D.-E.,  
23 Shaiganfar, R., Wagner, T., Merlaud, A., Van Roozendaal, M., Belegante, L., Nicolae, D.,  
24 Georgescu, L., and Burrows, J. P.: High-resolution airborne imaging DOAS measurements of NO<sub>2</sub>  
25 above Bucharest during AROMAT, *Atmos. Meas. Tech.*, 10, 1831-1857,  
26 <https://doi.org/10.5194/amt-10-1831-2017>, 2017.

1 Merlaud, A., Tack, F., Constantin, D., Georgescu, L., Maes, J., Fayt, C., Mingireanu, F.,  
2 Schuettmeyer, D., Meier, A. C., Schönardt, A., Ruhtz, T., Bellegante, L., Nicolae, D., Den Hoed,  
3 M., Allaart, M., and Van Roozendael, M.: The Small Whiskbroom Imager for atmospheric  
4 composition monitorinG (SWING) and its operations from an unmanned aerial vehicle (UAV)  
5 during the AROMAT campaign, *Atmos. Meas. Tech.*, 11, 551-567, [https://doi.org/10.5194/amt-](https://doi.org/10.5194/amt-11-551-2018)  
6 [11-551-2018](https://doi.org/10.5194/amt-11-551-2018), 2018.

7 Nowlan, C. R., Liu, X., Janz, S. J., Kowalewski, M. G., Chance, K., Follette-Cook, M. B., Fried,  
8 A., González Abad, G., Herman, J. R., Judd, L. M., Kwon, H.-A., Loughner, C. P., Pickering, K.  
9 E., Richter, D., Spinei, E., Walega, J., Weibring, P., and Weinheimer, A. J.: Nitrogen dioxide and  
10 formaldehyde measurements from the GEOstationary Coastal and Air Pollution Events (GEO-  
11 CAPE) Airborne Simulator over Houston, Texas, *Atmos. Meas. Tech. Discuss.*,  
12 <https://doi.org/10.5194/amt-2018-156>, in review, 2018.

13 Ortega, I., Koenig, T., Sinreich, R., Thomson, D., and Volkamer, R.: The CU 2-D-MAX-DOAS  
14 instrument – Part 1: Retrieval of 3-D distributions of NO<sub>2</sub> and azimuth-dependent OVOC ratios,  
15 *Atmos. Meas. Tech.*, 8, 2371-2395, <https://doi.org/10.5194/amt-8-2371-2015>, 2015.

16 Perner, D. and Platt, U.: Detection of nitrous acid in the atmosphere by differential optical  
17 absorption, *Geophys. Res. Lett.*, 6, 917–920, 1979.

18 Peters, E., Wittrock, F., Großmann, K., Frieß, U., Richter, A., and Burrows, J. P.: Formaldehyde  
19 and nitrogen dioxide over the remote western Pacific Ocean: SCIAMACHY and GOME-2  
20 validation using ship-based MAX-DOAS observations, *Atmospheric Chemistry and Physics*, 12,  
21 11179-11197, 2012.

22 Platt, U. and Stutz, J.: *Differential Optical Absorption Spectroscopy. Physics of Earth and Space*  
23 *Environments*, Springer, Berlin, 2008.

24 Richter, A., Burrows, J. P., Nüß, H., Granier, C., and Niemeier, U.: Increase in tropospheric  
25 nitrogen dioxide over China observed from space, *Nature*, 437, 129-132, DOI:  
26 [10.1038/nature04092](https://doi.org/10.1038/nature04092), 2005.

1 Richter, A., Begoin, M., Hilboll, A., and Burrows, J. P.: An improved NO<sub>2</sub> retrieval for the GOME-  
2 2 satellite instrument, *Atmos. Meas. Tech.*, 4, 1147-1159, doi:10.5194/amt-4-1147-2011, 2011.

3 Rivera, C., Sosa, G., Whrnshimmel, H., de Foy, B., Johansson, M., and Galle, B.: Tula  
4 industrial complex (Mexico) emissions of SO<sub>2</sub> and NO<sub>2</sub> during the MCMA 2006 field campaign  
5 using a mobile mini-DOAS system, *Atmos. Chem. Phys.*, 9, 6351–6361, doi:10.5194/acp-9-6351-  
6 2009, 2009.

7 Rivera, C., Barrera, H., Grutter, M., Zavala, M., Galle, B., Bei, N., Li, G., and Molina, L. T.: NO<sub>2</sub>  
8 fluxes from Tijuana using a mobile mini-DOAS during Cal-Mex 2010, *Atmos. Environ.*, 70, 532-  
9 539, 2013.

10 Roscoe, H. K., Van Roozendaal, M., Fayt, C., du Piesanie, A., Abuhassan, N., Adams, C., Akrami,  
11 M., Cede, A., Chong, J., Clémer, K., Friess, U., Gil Ojeda, M., Goutail, F., Graves, R., Griesfeller,  
12 A., Grossmann, K., Hemerijckx, G., Hendrick, F., Herman, J., Hermans, C., Irie, H., Johnston, P.  
13 V., Kanaya, Y., Kreher, K., Leigh, R., Merlaud, A., Mount, G. H., Navarro, M., Oetjen, H.,  
14 Pazmino, A., Perez-Camacho, M., Peters, E., Pinardi, G., Puentedura, O., Richter, A., Schönhardt,  
15 A., Shaiganfar, R., Spinei, E., Strong, K., Takashima, H., Vlemmix, T., Vrekoussis, M., Wagner,  
16 T., Wittrock, F., Yela, M., Yilmaz, S., Boersma, F., Hains, J., Kroon, M., Piders, A., and Kim, Y.  
17 J.: Intercomparison of slant column measurements of NO<sub>2</sub> and O<sub>4</sub> by MAX-DOAS and zenith-sky  
18 UV and visible spectrometers, *Atmos. Meas. Tech.*, 3, 1629-1646, doi:10.5194/amt-3-1629-2010,  
19 2010.

20 Rothman, L. S., Barbe, A., Benner, D. C., Brown, L. R., Camy-Peyret, C., Carleer, M. R., Chance,  
21 K., Clerbaux, C., Dana, V., Devi, V. M., Fayt, A., Flaud, J.-M., Gamache, R. R., Goldman, A.,  
22 Jacquemart, D., Jucks, K. W., Lafferty, W. J., Mandin, J.-Y., Massie, S. T., Nemtchinov, V.,  
23 Newnham, D. A., Perrin, A., Rinsland, C. P., Schroeder, J., Smith, K. M., Smith, M. A. H., Tang,  
24 K., Toth, R. A., Auwera, J. V., Varanasi, P., and Yoshino, K.: The HITRAN molecular  
25 spectroscopic database: edition of 2000 including updates through 2001, *J. Quant. Spectr. Rad.*  
26 *Transf.*, 82, 5–44, 2003.

1 Rozanov, V., Rozanov, A., Kokhanovsky, A., and Burrows, J.: Radiative transfer through  
2 terrestrial atmosphere and ocean: Software package SCIATRAN, *J. Quant. Spec. R.*  
3 *Trans.*, doi: 10.1016/j.jqsrt.2013.07.004, 2014.

4 Schönhardt, A., Altube, P., Gerilowski, K., Krautwurst, S., Hartmann, J., Meier, A. C., Richter, A.,  
5 and Burrows, J. P.: A wide field-of-view imaging DOAS instrument for two-dimensional trace gas  
6 mapping from aircraft, *Atmos. Meas. Tech.*, 8, 5113-5131, doi:10.5194/amt-8-5113-2015, 2015.

7 Schreier, S. F., Peters, E., Richter, A., Lampel, J., Wittrock, F., and Burrows, J. P.: Ship-based  
8 MAX-DOAS measurements of tropospheric NO<sub>2</sub> and SO<sub>2</sub> in the South China and Sulu Sea,  
9 *Atmos. Environ.*, 102, 331–343, doi:10.1016/j.atmosenv.2014.12.015, 2015.

10 Schreier, S. F., Richter, A., Wittrock, F., and Burrows, J. P.: Estimates of free-tropospheric NO<sub>2</sub>  
11 and HCHO mixing ratios derived from high-altitude mountain MAX-DOAS observations at  
12 midlatitudes and in the tropics, *Atmos. Chem. Phys.*, 16, 2803-2817, [https://doi.org/10.5194/acp-](https://doi.org/10.5194/acp-16-2803-2016)  
13 [16-2803-2016](https://doi.org/10.5194/acp-16-2803-2016), 2016.

14 Serdyuchenko, A., Gorshelev, V., Weber, M., Chehade, W., and Burrows, J. P.: High spectral  
15 resolution ozone absorption cross-sections – Part 2: Temperature dependence, *Atmos. Meas. Tech.*,  
16 7, 625-636, doi:10.5194/amt-7-625-2014, 2014.

17 Seyler, A., Wittrock, F., Kattner, L., Mathieu-Üffing, B., Peters, E., Richter, A., Schmolke, S., and  
18 Burrows, J. P.: Monitoring shipping emissions in the German Bight using MAX-DOAS  
19 measurements, *Atmos. Chem. Phys.*, 17, 10997-11023, [https://doi.org/10.5194/acp-17-10997-](https://doi.org/10.5194/acp-17-10997-2017)  
20 [2017](https://doi.org/10.5194/acp-17-10997-2017), 2017.

21 Shaiganfar, R., Beirle, S., Sharma, M., Chauhan, A., Singh, R. P., and Wagner, T.: Estimation of  
22 NO<sub>x</sub> emissions from Delhi using Car MAX-DOAS observations and comparison with OMI  
23 satellite data, *Atmos. Chem. Phys.*, 11, 10871-10887, doi:10.5194/acp-11-10871-2011, 2011.

24 Sinnhuber, B.-M., Weber, M., Amankwah, A., and Burrows, J. P.: Total ozone during the unusual  
25 Antarctic winter of 2002, *Geophys. Res. Lett.*, 30, 1580–1584, doi:10.1029/2002GL016798,  
26 2003a.



1 Sinnhuber, M., Burrows, J. P., Chipperfield, M. P., Jackman, C. H., Kallenrode, M.-B., Künzi, K.  
2 F., and Quack, M.: A model study of the impact of magnetic field structure on atmospheric  
3 composition during solar proton events, *Geophys. Res. Lett.*, 30, 1818–1821,  
4 doi:10.1029/2003GL017265, 2003b.

5 Sinreich, R., Merten, A., Molina, L., and Volkamer, R.: Parameterizing radiative transfer to  
6 convert MAX-DOAS dSCDs into near-surface box-averaged mixing ratios, *Atmos. Meas. Tech.*,  
7 6, 1521–1532, <https://doi.org/10.5194/amt-6-1521-2013>, 2013.

8 Spangl, W. and Nagl, C.: Jahresbericht der Luftgütemessungen in Österreich 2015, REPORT REP-  
9 0562, Umweltbundesamt GmbH, Wien, 2016.

10 [Spangl, W.: Luftgütemessstellen in Österreich, REPORT REP 0607, Umweltbundesamt GmbH,](#)  
11 [Wien, 2017.](#)

12 [Tack, F., Hendrick, F., Goutail, F., Fayt, C., Merlaud, A., Pinaridi, G., Hermans, C., Pommereau,](#)  
13 [J.-P., and Van Roozendaal, M.: Tropospheric nitrogen dioxide column retrieval from ground-based](#)  
14 [zenith-sky DOAS observations, \*Atmos. Meas. Tech.\*, 8, 2417-2435, \[https://doi.org/10.5194/amt-\]\(https://doi.org/10.5194/amt-8-2417-2015\)](#)  
15 [8-2417-2015, 2015.](#)

16 Tack, F., Merlaud, A., Iordache, M.-D., Danckaert, T., Yu, H., Fayt, C., Meuleman, K., Deutsch,  
17 F., Fierens, F., and Van Roozendaal, M.: High-resolution mapping of the NO<sub>2</sub> spatial distribution  
18 over Belgian urban areas based on airborne APEX remote sensing, *Atmos. Meas. Tech.*, 10, 1665-  
19 1688, <https://doi.org/10.5194/amt-10-1665-2017>, 2017.

20 Takashima, H., Irie, H., Kanaya, Y., and Syamsudin, F.: NO<sub>2</sub> observations over the western Pacific  
21 and Indian Ocean by MAX-DOAS on Kaiyo, a Japanese research vessel, *Atmospheric*  
22 *Measurement Techniques*, 5, 2351-2360, 2012.

23 Thalman, R. and Volkamer, R.: Temperature dependent absorption cross-sections of O<sub>2</sub>-O<sub>2</sub>  
24 collision pairs between 340 and 630 nm and at atmospherically relevant pressure., *Phys. Chem.*  
25 *Chem. Phys.*, 15, 15371–15381, <https://doi.org/10.1039/c3cp50968k>, 2013.

1 Vandaele, A. C., Hermans, C., Simon, P. C., Roozendael, M. V., Guilmot, J. M., Carleer, M., and  
2 Colin, R.: Fourier transform measurement of NO<sub>2</sub> absorption cross-section in the visible range at  
3 room temperature, *J. Atmos. Chem.*, 25, 289–305, 1996.

4 Wagner, T., Ibrahim, O., Shaiganfar, R., and Platt, U.: Mobile MAX-DOAS observations of  
5 tropospheric trace gases, *Atmos. Meas. Tech.*, 3, 129-140, doi:10.5194/amt-3-129-2010, 2010.

6 Wang, P., Richter, A., Bruns, M., Rozanov, V. V., Burrows, J. P., Heue, K.-P., Wagner, T., Pundt,  
7 I., and Platt, U.: Measurements of tropospheric NO<sub>2</sub> with an airborne multi-axis DOAS instrument,  
8 *Atmos. Chem. Phys.*, 5, 337–343, doi:10.5194/acp-5-337-2005, 2005.

9 Wang, S., Zhou, B., Wang, Z., Yang, S., Hao, N., Valks, P., Trautmann, T., and Chen, L.: Remote  
10 Sensing of NO<sub>2</sub> Emission from the Central Urban Area of Shanghai (China) Using the Mobile  
11 DOAS Technique. *Journal of Geophysical Research*, 117 (D13305), doi:10.1029/2011JD016983,  
12 2012.

13 WHO: Health Aspects of Air Pollution with Particulate Matter, Ozone and Nitrogen Dioxide,  
14 World Health Organization, Bonn, 2003.

15 Winkler, H., Sinnhuber, M., Notholt, J., Kallenrode, M.-B., Steinhilber, F., Vogt, J., Zieger, B.,  
16 Glassmeier, K.-H., and Stadelmann, A.: Modeling impacts of geomagnetic field variations on  
17 middle atmospheric ozone responses to solar proton events on long timescales, *J. Geophys. Res.*,  
18 113, 11 pp., D02302, doi:10.1029/2007JD008574, 2008.

19 Wittrock, F., Oetjen, H., Richter, A., Fietkau, S., Medeke, T., Rozanov, A., and Burrows, J. P.:  
20 MAX-DOAS measurements of atmospheric trace gases in Ny-Ålesund – Radiative transfer studies  
21 and their application, *Atmos. Chem. Phys.*, 4, 955–966, doi:10.5194/acp-4-955-2004, 2004.

22 Wu, F. C., Xie, P. H., Li, A., Chan, K. L., Hartl, A., Wang, Y., Si, F. Q., Zeng, Y., Qin, M., Xu, J.,  
23 Liu, J. G., Liu, W. Q., and Wenig, M.: Observations of SO<sub>2</sub> and NO<sub>2</sub> by mobile DOAS in the  
24 Guangzhou eastern area during the Asian Games 2010, *Atmos. Meas. Tech.*, 6, 2277-2292,  
25 doi:10.5194/amt-6-2277-2013, 2013.

26 [www.doas-vindobona.at](http://www.doas-vindobona.at)

1 [www.donauturm.at](http://www.donauturm.at)

2 [www.statistik.at](http://www.statistik.at)

3 [www.tropomi.eu/data-products/cindi-2](http://www.tropomi.eu/data-products/cindi-2)

4 [www.vcoe.at](http://www.vcoe.at)

5

6

7

8

9

10

11

12 **Table 1.** Technical characteristics of the DOAS instrument.

**AvaSpec-ULS2048x64**

<u>spectral range</u>	<u>spectral resolution</u>	<u>optical fibres</u>				
<u>300-550 nm</u>	<u>0.65 nm</u>	<u>quartz fibre bundle</u>				
<u>type of application</u>	<u>elevation angle</u>	<u>field of view</u>	<u>typical exposure time</u>	<u>averaging time</u>	<u>dark signal</u>	<u>line shape</u>
<u>car DOAS zenith-sky</u>	<u>90°</u>	<u>approx. ± 5°</u>	<u>0.025 seconds</u>	<u>5 seconds</u>	<u>before / after measurements</u>	<u>HgCd lamp</u>
<u>tower DOAS off-axis</u>	<u>0°</u>	<u>approx. 1° (focused by lens)</u>		<u>10 seconds</u>		

13

14

15

16

17

1  
2  
3  
4  
5  
6  
7  
8  
9  
10  
11  
12  
13  
14  
15  
16  
17  
18

**Table 2.** DOAS settings for the retrieval of NO<sub>2</sub>.

Fit parameter		Selection/Source
Spectral range		425-490 nm
Polynomial degree		5 (car zenith-sky), 7 (tower off-axis)
Wavelength calibration		Solar atlas (Kurucz et al., 1984)
Reference		Zenith-sky spectrum (close to noontime) <sup>a, b, c</sup>
Cross section	Temperature	Data source
O <sub>3</sub>	223 K	Serdyuchenko et al. (2014) with I <sub>0</sub> correction
NO <sub>2</sub>	298 K	Vandaele et al. (1996) with I <sub>0</sub> correction
O <sub>4</sub>	293 K	Thalman and Volkamer (2013)
H <sub>2</sub> O	-	Rothmann et al. (2010)
Ring	-	QDOAS (Danckert et al., 2015)

<sup>a</sup> Reference measurement for the retrieval of DSCD<sub>meas</sub> on 10 April 2015 was taken on 10 April 2015 at 10:49 UT (48° 17' 52.08'' N, 16° 33' 44.64'' E).  
<sup>b</sup> Reference measurement for the retrieval of DSCD<sub>meas</sub> on 27 September, 28 September, 2 October, and 6 October 2015 was taken on 27 September 2015 at 10:17 UT (48° 21' 52.75'' N, 16° 31' 20.24'' E).

Formatted

<sup>c</sup> Reference measurement for the retrieval of DSCD<sub>meas</sub> on 19 October, 23 October, 27 October, and 3 November 2015 was taken on 23 October 2015 at 10:14 UT (48° 21' 53.85" N, 16° 31' 22.48" E).

**Table 23.** Summary of statistics of the individual car journeys including lap averages of wind speed, wind direction, temperature, pressure, number density of air, mixing-height, in-situ NO<sub>2</sub> from selected air quality monitoring stations, and NO<sub>2</sub> VCD<sub>tropo</sub> from car DOAS measurements. Converted averaged NO<sub>2</sub> mixing ratios for both measurements are also given. The correlation coefficients (R) obtained from the linear relationship between car DOAS and in situ NO<sub>2</sub> are also shown (further details are given in the text).

	10.04.2015 <sup>a</sup> 2015			27.09.2015 <sup>b</sup> 2015		28.09.2015 <sup>b,2</sup>	Formate
Car journey (UT)	05:27-06:59	07:06-08:35	08:40-10:04	07:11-08:42	08:42-10:17	06:36-08:20	08:21-10:05
Wind speed [km h <sup>-1</sup> ] <sup>d, a</sup>	3.9±2.4	5.4±2.8	6.7±2.4	14.4±4.9	15.3±5.4	16.1±5	19.8±6.4
Wind direction [deg] <sup>d, a</sup>	135.5±29.6	126.2±29.3	114.1±24.6	337.2±7.1	240.3±81.5	187.1±114.2	91.7±99.4
Temperature [°C] <sup>e, b</sup>	7.4±1	10.4±0.8	13±0.7	12.6±0.3	13.7±0.4	12.4±0.6	14.2±0.5
Pressure [hPa] <sup>e, b</sup>	994.6±0.1	994.7±0	994.5±0	996.1±0.3	996.5±0.1	1000.6±0.2	1000.7±0.1
Number density of air [molec cm <sup>-3</sup> ] <sup>f</sup>	2.568e+19	2.541e+19	2.517e+19	2.525e+19	2.516e+19	2.538e+19	2.522e+19

Mixing-height [m] <sup>e,d</sup>	148.2±28.6	311.7±46.4	445.7±30.1	1103.7±50.2	1045.4±30	541.3±105.9	11
In situ NO <sub>2</sub> [μg m <sup>-3</sup> ] <sup>h,c</sup>	63.3±22.9	43.7±23	35.5±20.3	9.3±5.2	8.4±4.5	20.4±11.7	0
In situ X <sub>NO<sub>2</sub></sub> [ppb] <sup>i,f</sup>	31.6±11.4	22.0±11.6	18.1±10.3	4.7±2.7	4.3±2.3	10.3±5.9	0
Car DOAS NO <sub>2</sub> [10 <sup>16</sup> molec cm <sup>-2</sup> ] <sup>j,g</sup>	1.3406±0.4938	1.02±0.4991±0.43	0.9489±0.7472	0.2321±0.0908	0.15±0.09	0.4236±0.1814	0
Car DOAS (BL) X <sub>NO<sub>2</sub></sub> [ppb] <sup>h</sup>	35.2±1227.8±9.9	12.9±6.211.5±5.4	8.4±7.9±6.64	0.87±0.3	0.6±0.43	32.6±1.3	0
Car DOAS (Surface) X <sub>NO<sub>2</sub></sub> [ppb] <sup>i</sup>	26.21	21.58	18.5	7.3	6.52	11	0
Correlation coefficient <sup>m</sup> coefficient <sup>j</sup>		0.8083		0.3738		0.65	

1

2 **Table 23.** continued.

	02.10.2015 <sup>b</sup> 2015			06.10.2015 <sup>b</sup> 2015		19.10.2015 <sup>b</sup> 20	
Car journey (UT)	05:22-06:58	07:01-08:29	08:29-09:55	06:57-08:23	08:24-09:57	06:57-08:30	08
Wind speed [km h <sup>-1</sup> ] <sup>d,a</sup>	4.7±2.1	10.9±2.9	16.9±4.5	8.1±3.3	10±3.1	8.1±2.9	3
Wind direction [deg] <sup>d,a</sup>	125.3±40.3	134.8±6.9	139.8±5.8	120.4±7.7	122.8±11.6	293.3±23.4	3
Temperature [°C] <sup>e,b</sup>	7.7±1.3	11.1±1.2	14.8±0.9	12.9±1	14.7±0.2	7.7±0.2	9
Pressure [hPa] <sup>e,b</sup>	997.6±0.1	997.5±0	997±0.2	982±0	981.9±0.1	987±0.1	9
Number density of air [molec cm <sup>-3</sup> ] <sup>f,c</sup>	2.573e+19	2.542e+19	2.508e+19	2.471e+19	2.486e+19	2.545e+19	2
Mixing-height [m] <sup>e,d</sup>	206.8±51.6	350.4±44.5	666.9±136.2	381.6±24.8	480.4±34.4	412.4±23.2	37
In situ NO <sub>2</sub> [μg m <sup>-3</sup> ] <sup>h,c</sup>	44.1±17.3	27.2±10	19.9±12.6	27.3±9	25.4±10.2	30.8±10.9	3
In situ X <sub>NO<sub>2</sub></sub> [ppb] <sup>i,f</sup>	22±8.6	13.7±5	10.1±6.4	14.1±4.6	13.2±5.3	15.5±5.5	1
Car DOAS NO <sub>2</sub> [10 <sup>16</sup> molec cm <sup>-2</sup> ] <sup>j,g</sup>	0.7458±0.4836	0.474±0.3527	0.2423±0.218	0.6554±0.4131	0.5549±0.3732	0.5347±0.3528	0.5
Car DOAS (BL) X <sub>NO<sub>2</sub></sub> [ppb] <sup>h</sup>	1310.9±96.8	4.5±3±3.9.1	1.54±1.21	5.6.8±4.2±3.3	4.5±3.1±2.7	5.1±3.4.4±2.6	5.2
Car DOAS (Surface) X <sub>NO<sub>2</sub></sub> [ppb] <sup>i</sup>	23.43	+615.7	7.42	13.73	12.23	17.6	0
Correlation coefficient <sup>m</sup> coefficient <sup>j</sup>		0.73		0.7879		0.23	

3

4 **Table 23.** continued.

	23.10.2015 <sup>b</sup> 2015		27.10.2015 <sup>b</sup> 2015		03.11.2015 <sup>b</sup> 2015		
Car journey (UT)	06:58-08:46	08:47-10:14	06:58-08:37	08:37-10:02	06:44-08:15	08:15-09:43	
Wind speed [km h <sup>-1</sup> ] <sup>d,a</sup>	13.8±4	14±4.2	16±5	19±5.2	8.2±3.2	9.9±3.7	
Wind direction [deg] <sup>d,a</sup>	282.6±8	294.5±9.5	134±7.2	137.1±6.7	152.1±31	157.2±20.9	
Temperature [°C] <sup>e,b</sup>	10±0.3	11.1±0.4	9±0.2	10.6±1	3±0.4	4.2±0.4	
Pressure [hPa] <sup>e,b</sup>	991.3±0.4	992±0.1	991.6±0.1	991.7±0.1	995.7±0.1	995.4±0.1	
Number density of air [molec cm <sup>-3</sup> ] <sup>f</sup>	2.536e+19	2.528e+19	2.545e+19	2.531e+19	2.611e+19	2.599e+19	
Mixing-height [m] <sup>e,d</sup>	357.5±24.1	482.3±50	460±14.7	631.2±79.7	417.4±8.1	471.2±25.7	
In situ NO <sub>2</sub> [μg m <sup>-3</sup> ] <sup>h,c</sup>	26.3±8.2	25.4±7.9	22.8±10.3	18.8±8.6	52.7±19.6	36.6±18.2	
In situ X <sub>NO<sub>2</sub></sub> [ppb] <sup>i,f</sup>	13.3±4.2	12.8±4	11.5±5.2	9.5±4.3	25.9±9.6	18.1±9	
Car DOAS NO <sub>2</sub> [10 <sup>16</sup> molec cm <sup>-2</sup> ] <sup>j,g</sup>	1.4413±0.538	1±0.5187±0.4	0.2726±0.151	0.23±0.1412	0.8873±0.513	0.7263±0.473	
Car DOAS (BL) X <sub>NO<sub>2</sub></sub> [ppb] <sup>h</sup>	1512.5±5.54	2	2	2	8	8	
Car DOAS (Surface) X <sub>NO<sub>2</sub></sub> [ppb] <sup>i</sup>	2	8.2±4.7.1±3.5	2.32±1.3	1.5±0.97	8±46.7±3.6	5.92±3.81	

46

Car DOAS (Surface) X <sub>NO2</sub> [ppb] <sup>i</sup>	17.1	14.34	11.5	7.46	23.31	20.35
Correlation coefficient <sup>m</sup>	0.07		0.72		0.9493	

<sup>a</sup>Reference measurement taken on 10 April 2015 at 10:49 UT (48° 17' 52.08" N, 16° 33' 44.64" E).

<sup>b</sup>Reference measurement taken on 27 September 2015 at 10:17 UT (48° 21' 52.75" N, 16° 31' 20.24" E).

<sup>c</sup>Reference measurement taken on 23 October 2015 at 10:14 UT (48° 21' 53.85" N, 16° 31' 22.48" E).

<sup>da</sup>Measurements from 9 stations are provided by ZAMG. Values represent lap averages and standard deviations.

<sup>db</sup>Measurements provided by the BOKU weather station. Values represent lap averages and standard deviations.

<sup>dc</sup>Calculations are based on the relationship between pressure and temperature measurements. Values represent lap averages.

<sup>dd</sup>Measurements provided by ZAMG. Values represent lap averages and standard deviations.

<sup>de</sup>Measurements from 15 stations provided by UBA. Values represent lap averages and standard deviations.

<sup>df</sup>Conversion of mass concentrations into mixing ratios is based on Eq. 5.

<sup>dg</sup>Conversion of DSCD<sub>meas</sub> into VCD<sub>tropo</sub> is based on Eq. 1.

<sup>dh</sup>Conversion of VCD<sub>tropo</sub> into boundary layer mixing ratios is based on Eq. 3.

<sup>di</sup>Conversion of VCD<sub>tropo</sub> into surface mixing ratios is based on Eq. 4.

<sup>dj</sup>Values represent correlation coefficients between in situ NO<sub>2</sub> [ppb] and Car DOAS (BL) NO<sub>2</sub> [ppb].

**Table 4.** Parameter settings used for the simulation of tropospheric air mass factors with the radiative transfer model SCIATRAN.

Lower Austria		SCIATRAN input					
RTM mode	Klosterneuburg (Wiener Straße)	Klosterneuburg (Danubiasse)	Mannswörth	Schwechat	Vösendorf	Wolkersdorf	Gänserndorf
-RTM type	spherical atmosphere, multiple scattering	gas (se)					

Latitudes	Wa	48° 18' 10"	48° 08' 42"	48° 08' 45"	48° 07' 32"	48° 23' 32"	48° 20' 05"	
Wavelength		461 nm						
Longitudes	A				16° 28' 37"	16° 19' 60"	16° 31' 20"	16° 43' 50"
erosol								
Optical				16°				
Depth				19'	16°			
(AOD)		0.1, 0.25, 0.4		17"	30'			
-Single				E	40"	E		
scattering								
albedo								
(SSA)	Vienna	0.9, 0.95, 1.0						
	A23	Henyey-Greenstein	Belgradplatz	Floridsdorf	Kaiserebersdorf	Laaer Berg	Liesing	Lobau
Phase		asymmetry						
function		factor 0.7						
-Clouds	(Wehlistraße)	no clouds						
Latitudes	Sur		48° 10' 30"	48° 15' 42"	48° 09' 41"	48° 08' 17"	48° 09' 45"	48° 13' 37"
face			N	N	N	N	N	N
albedo		0.1						
					16° 23' 53"	16° 28' 38"	16° 23' 39"	16° 17' 48"
					E	E	E	E
								1
								6
								2
								7
								3
								3
								1
								1
								E
Profile		well-mixed within 300 m, 650 m, 1000 m						

1 **Table 3.** Overview on selected air quality monitoring stations, operated by the Environment  
2 Agency Austria.

- 3
- 4
- 5
- 6
- 7
- 8
- 9



1  
2  
3  
4  
5  
6  
7  
8  
9  
10  
11  
12  
13  
14  
15  
16  
17  
18  
19  
20

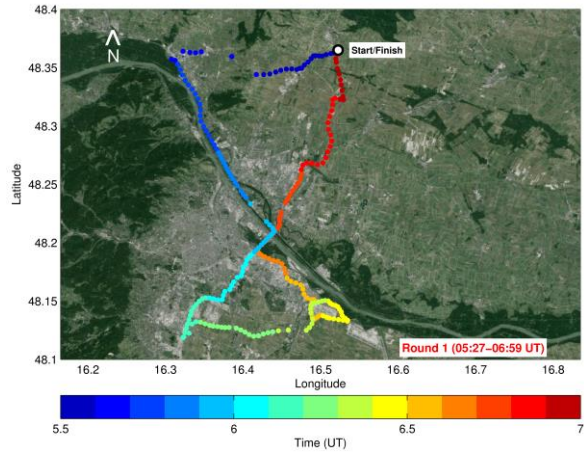
**Table 5.**

1 **Table 4.** Overview on selected meteorological stations, operated by the Austrian official weather  
2 service.

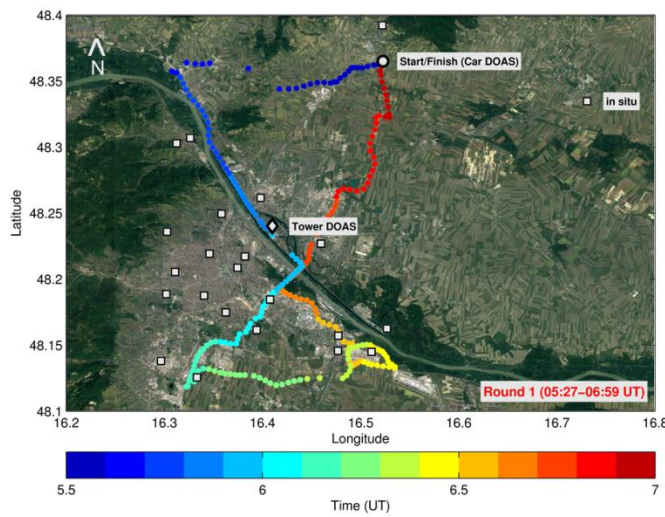
Lower Austria					
	Brunn am Gebirge	Gänserndorf	Gross-Enzersdorf	Wolkersdorf	
	(Stadt)				
Latitudes	48° 06' 25'' N	48° 20' 16'' N	48° 11' 59'' N	48° 22' 49'' N	
Longitudes	16° 16' 12'' E	16° 42' 49'' E	16° 33' 33'' E	16° 30' 27'' E	
Vienna					
	Donaufeld	Hohe Warte	Innere Stadt	Stammersdorf	Unterlaa
Latitudes	48° 15' 27'' N	48° 14' 55'' N	48° 11' 54'' N	48° 18' 21'' N	48° 07' 30'' N
Longitudes	16° 26' 00'' E	16° 21' 23'' E	16° 22' 01'' E	16° 24' 20'' E	16° 25' 10'' E

3  
4  
5  
6  
7  
8  
9  
10  
11

Formate



1



2

3 **Figure 1.** An Overview map with an example of a single car journey (color-coded dots) as  
 4 performed on 10 April 2015 between 05:27 and 06:59 UT. The locations of Start/Finish of the car  
 5 journeys, Danube Tower, and in situ measurement stations are shown by a circle, diamond, and  
 6 squares, respectively.

7

8

9

10

11

1  
2  
3  
4  
5  
6  
7  
8  
9  
10  
11  
12  
13  
14  
15  
16  
17  
18  
19

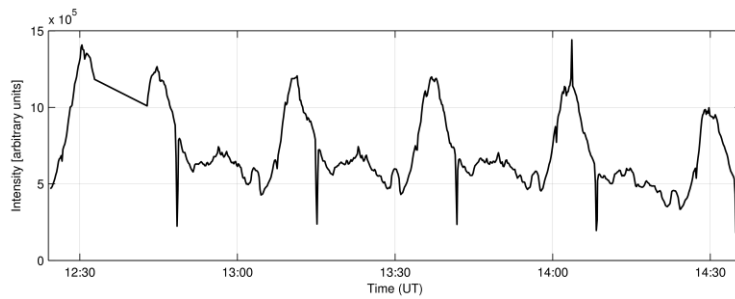
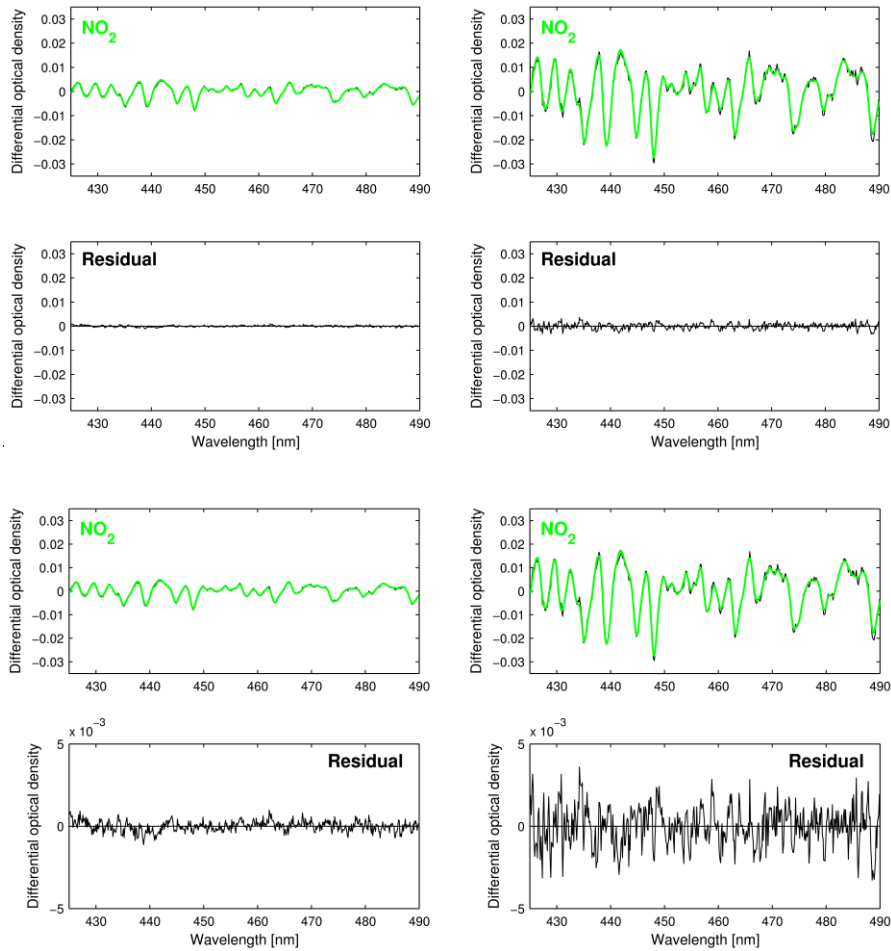


**Figure 2.** An example of a time series of the intensity of the spectrum as measured with the DOAS instrument from the rotating tower platform on 22 April 2016 between 12:25 and 14:35 UT. The sharp dips indicate a decrease in intensity due to pointing towards a skyscraper, which blocks the view of the instruments.

1



2

3

4 **Figure 3.** Exemplary fit results from the DOAS analysis in the 425-490 nm fitting window for a  
5 car DOAS spectrum (left panels), as measured on 10 April 2015 (SZA = 47.68°, DSCD = 4.03 x  
6 10<sup>16</sup> molec cm<sup>-2</sup>) and averaged over intervals of 5 seconds as well as exemplary fit results for a  
7 tower DOAS spectrum (right panels), as measured on 29 April 2016 (SZA = 66.99°, DSCD =  
8 1.46 x 10<sup>17</sup> molec cm<sup>-2</sup>;) and averaged over intervals of 10 seconds.

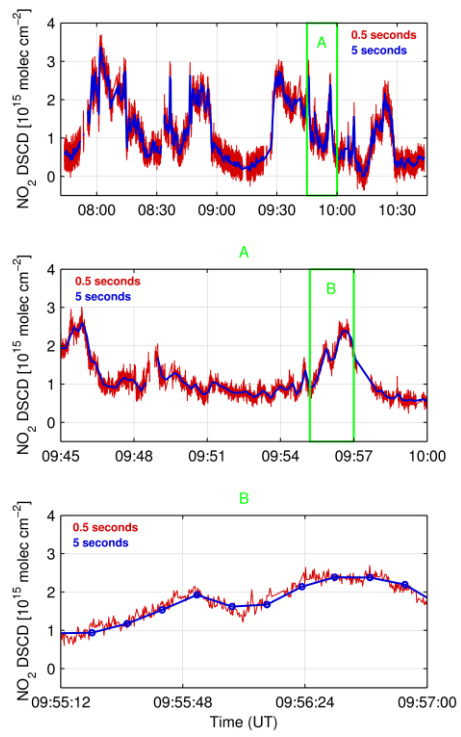
9

10

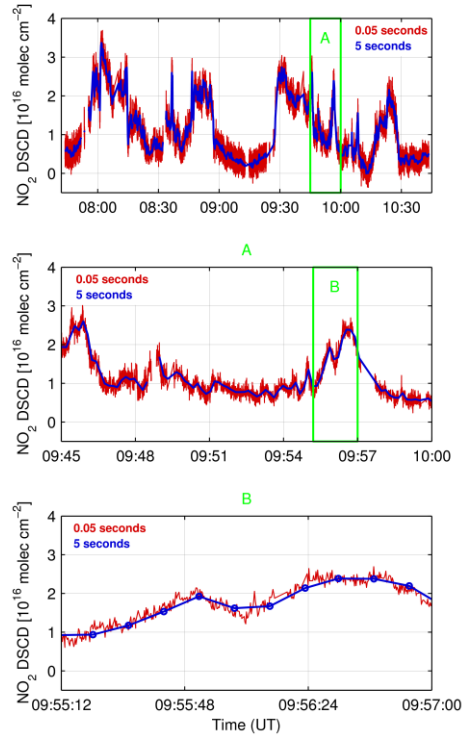
11

12

1  
2  
3  
4  
5  
6  
7  
8

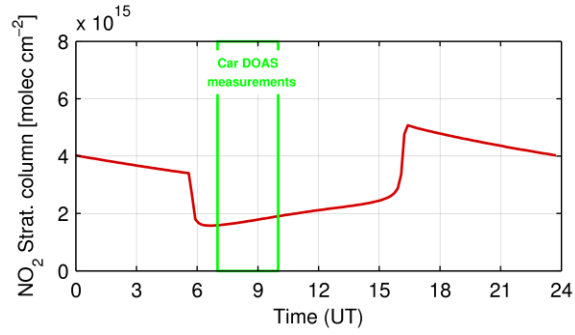


9



1  
 2 **Figure 4.** Temporal resolution of NO<sub>2</sub> DSCDs based on the car DOAS zenith-sky measurements  
 3 performed on 3 November 2015. The red and blue lines show data at a resolution of 0.505 and 5  
 4 seconds, respectively. The upper panel shows the NO<sub>2</sub> DSCDs for the whole period of  
 5 observations of that day, whereas the middle and lower panels represent shorter time sections for  
 6 clarity.

7  
 8  
 9  
 10  
 11  
 12  
 13



1

2 **Figure 5.** Stratospheric NO<sub>2</sub> above Vienna on 19 October 2014 (red line) as obtained from the  
3 Bremen 3d chemistry transport model (B3dCTM). The green rectangle indicates the time period  
4 of car DOAS measurements performed on that day.

5

6

7

8

9

10

11

12

13

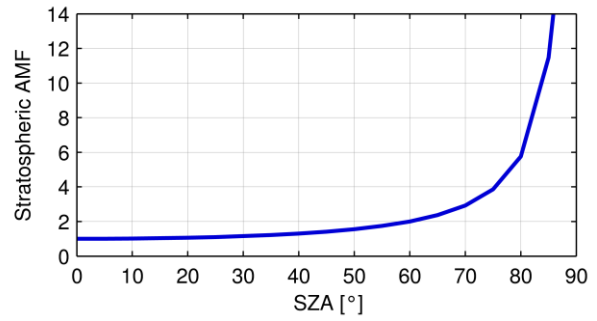
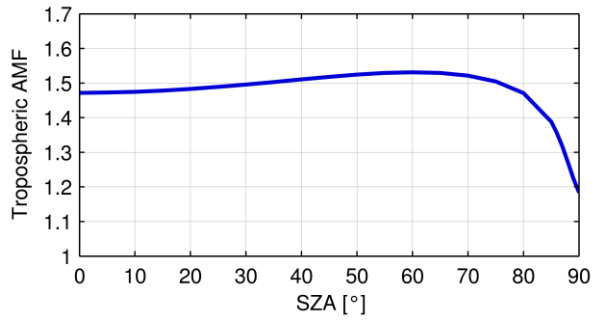
14

15

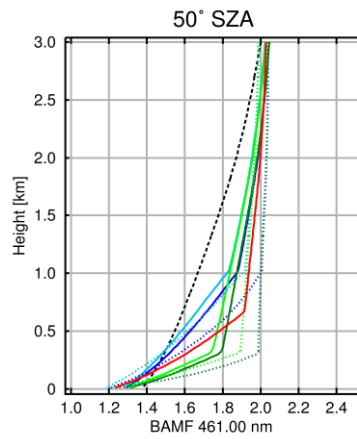
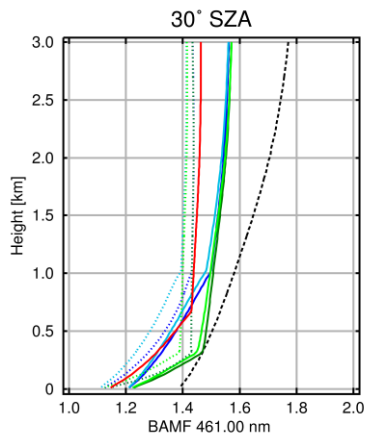
16

17

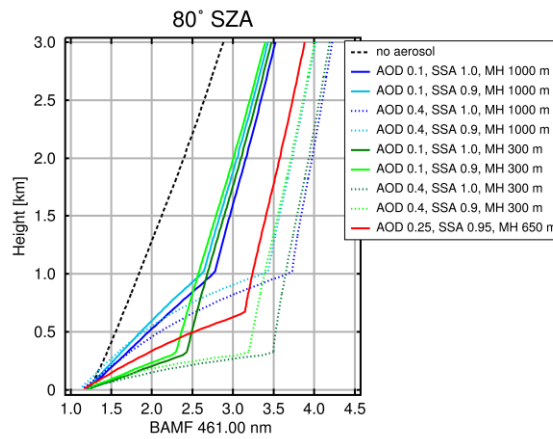
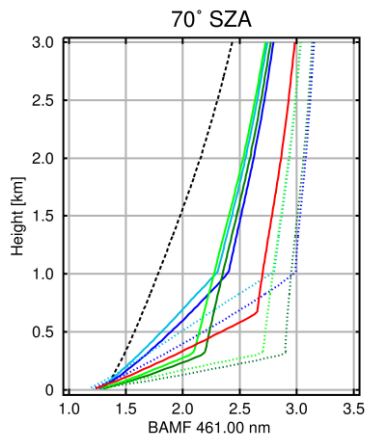




1  
2



3



4

5 **Figure 6.** Computed Simulated scenario-based tropospheric Box-AMFs for SZA = 30° (upper  
 6 left), SZA = 50° (upper right), SZA = 70° (lower left), and SZA = 80° (lower right). The red line  
 7 shows the Box-AMF that is based on an intermediate scenario. Other scenarios are indicated by  
 8 different colors and line styles.

1  
2  
3  
4  
5  
6  
7  
8  
9  
10  
11  
12  
13  
14  
15  
16  
17

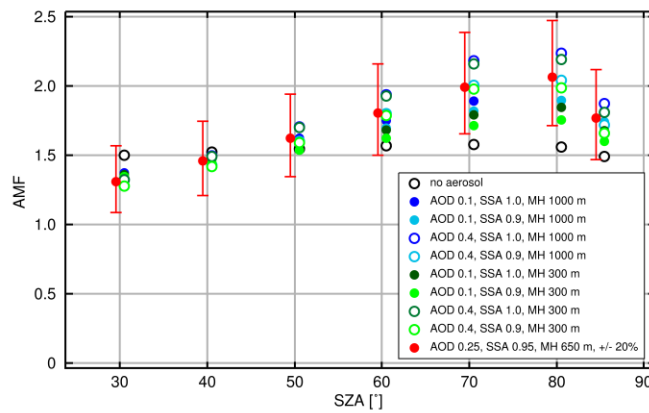


**Figure 7.** Simulated scenario-based tropospheric AMFs as a function of solar zenith angle for the troposphere (left) and stratosphere (right). SZA. The red dots represent the tropospheric AMFs that are used for the conversion of  $DSCD_{meas}$  into  $VCD_{tropo}$  in this study (see Eq. 1), error bars indicate  $\pm 20\%$ . The other scenarios are depicted by circles and dots.

1  
2  
3  
4  
5  
6  
7  
8  
9  
10  
11  
12  
13  
14  
15  
16  
17

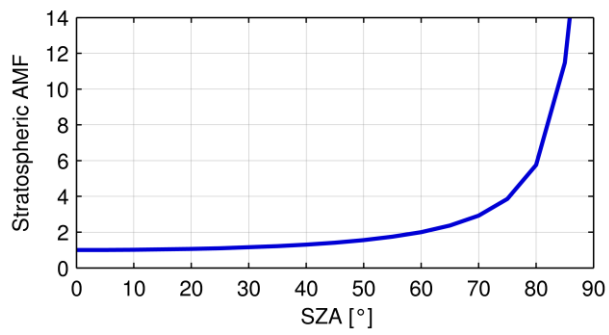
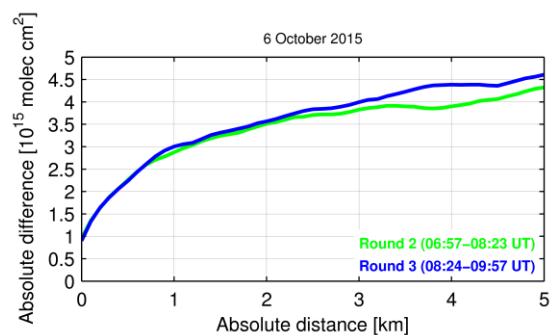
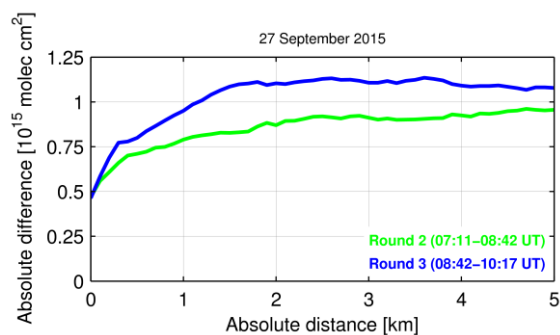


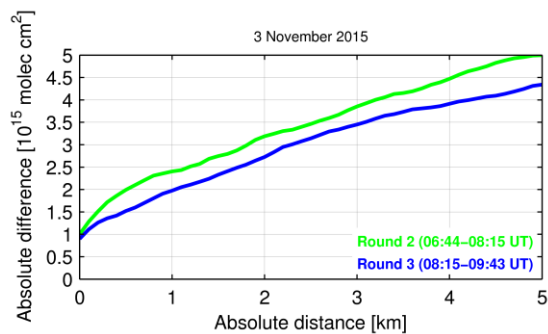
**Figure 8.** Simulated stratospheric AMFs as a function of SZA.

Formatte

1  
2  
3  
4  
5  
6



7

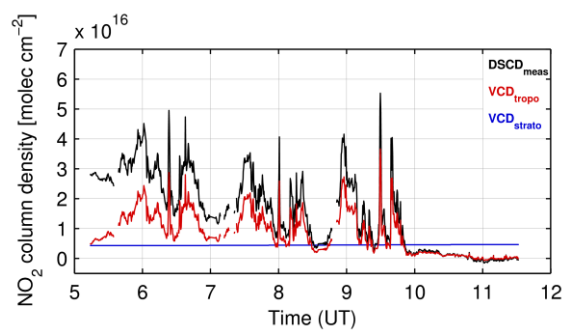


8

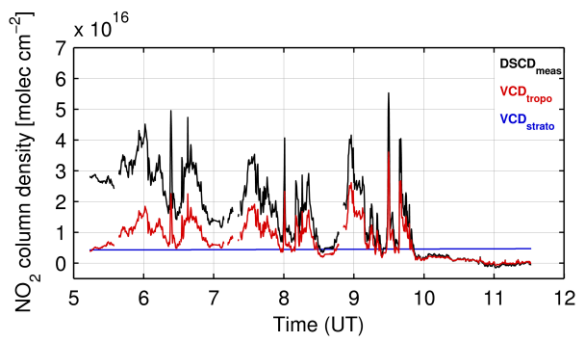
9 **Figure 79.** Mean absolute difference in  $\text{NO}_2$  DSCDs as a function of the absolute distance (see  
10 Sect. 3.2.1) for car DOAS zenith-sky measurements performed on three selected days with  
11 different wind conditions and  $\text{NO}_2$  levels.

12  
13  
14

1  
2  
3  
4  
5  
6



7

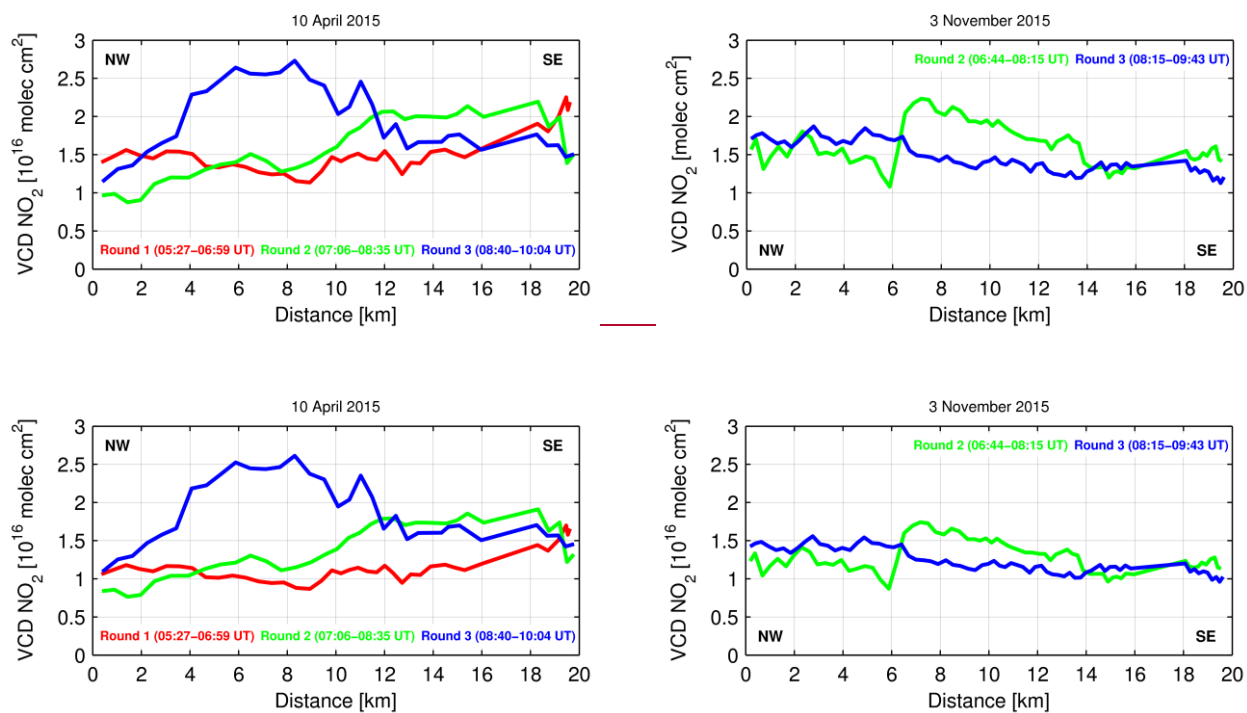


8

9 **Figure 810.** Time series of NO<sub>2</sub> DSCD<sub>meas</sub> (black), VCD<sub>tropo</sub> (red), and VCD<sub>strato</sub> (blue) obtained  
10 from car DOAS zenith-sky spectra recorded on 10 April 2015.

11  
12  
13  
14

1  
2  
3  
4  
5  
6  
7  
8

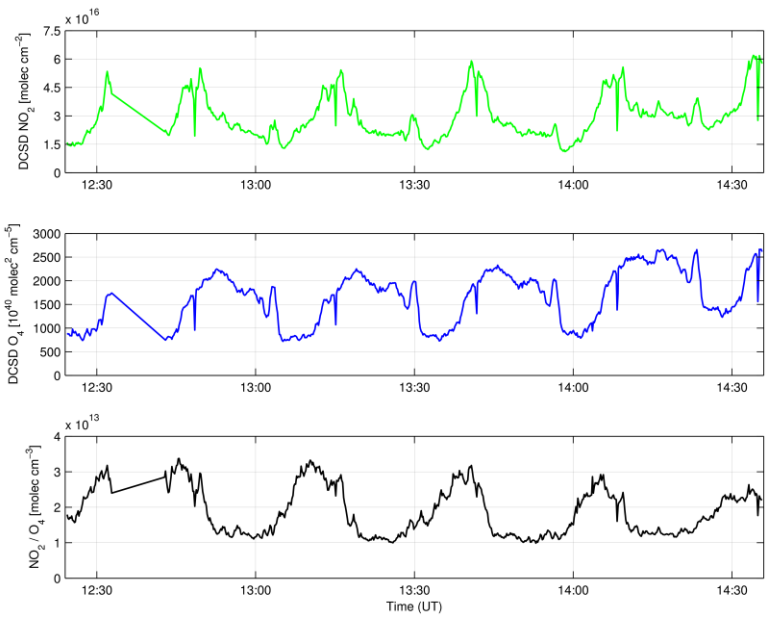


9  
10

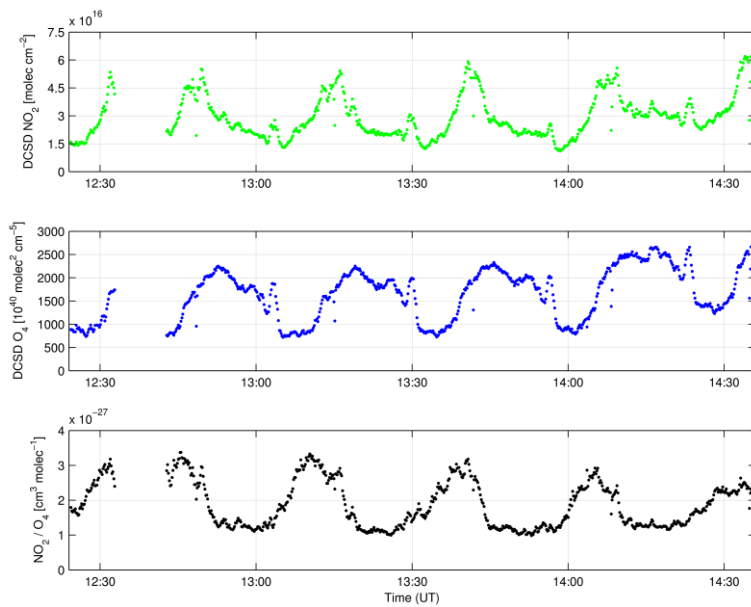
11 **Figure 911.** Temporal evolution of tropospheric NO<sub>2</sub> for the car DOAS zenith-sky measurements  
12 as performed on 10 April and 3 November 2015. The red, green, and blue curves represent NO<sub>2</sub>  
13 VCD<sub>tropo</sub> as obtained along the A22 during the first, second, and third journey, respectively.

14

1  
2  
3  
4  
5  
6  
7  
8  
9  
10  
11  
12  
13



14



1

2 **Figure 1012.** Time series of NO<sub>2</sub> (upper) and O<sub>4</sub> (middle) DSCDs as obtained from the tower  
 3 DOAS off-axis measurements performed on 22 April 2016. The ratio of NO<sub>2</sub>/O<sub>4</sub> is shown in the  
 4 lowest panel.

5

6

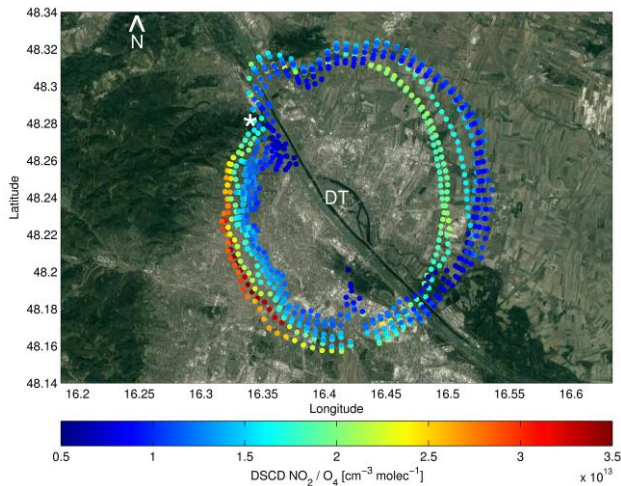
7

8

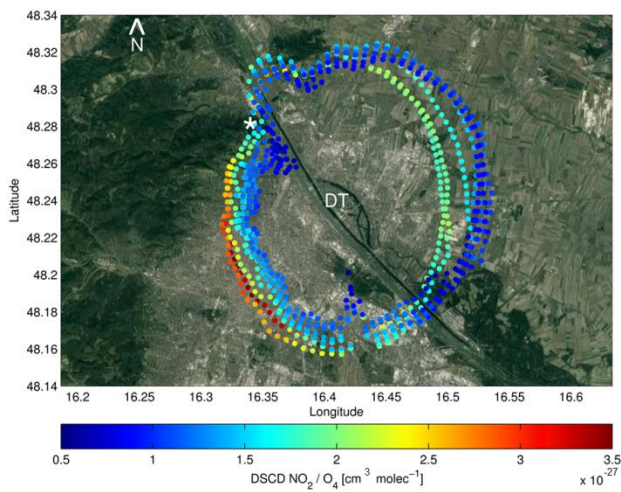
9

10





1



2

3 **Figure 113.** Spatial and temporal variability of the  $\text{NO}_2/\text{O}_4$  ratio (here, the radius is determined  
 4 by DSCD  $\text{O}_4$  values) on 10 May 2016 between 05:57 and 09:56 UT observed by tower DOAS  
 5 off-axis measurements. The position of the Vienna Danube Tower (DT) is highlighted in the  
 6 center of the geographical map. The white asterisk represents the summit of Kahlenberg (484 m  
 7 a.s.l.), which is used for the estimation of horizontal optical path lengths.

8

9

10

11

1

2

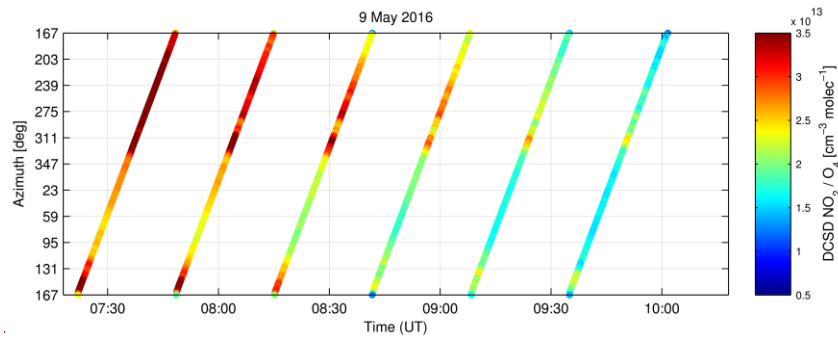
3

4

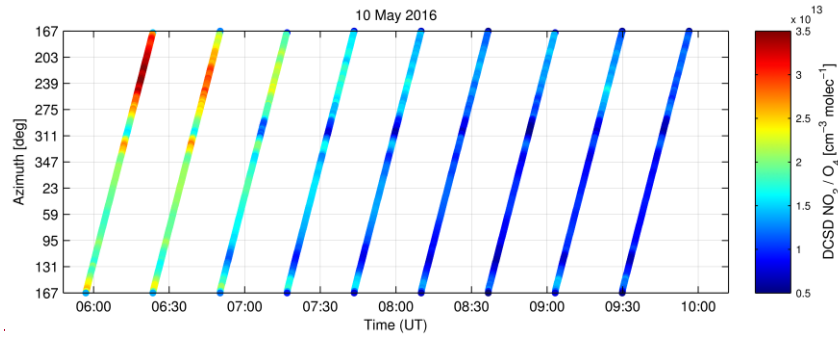
5

6

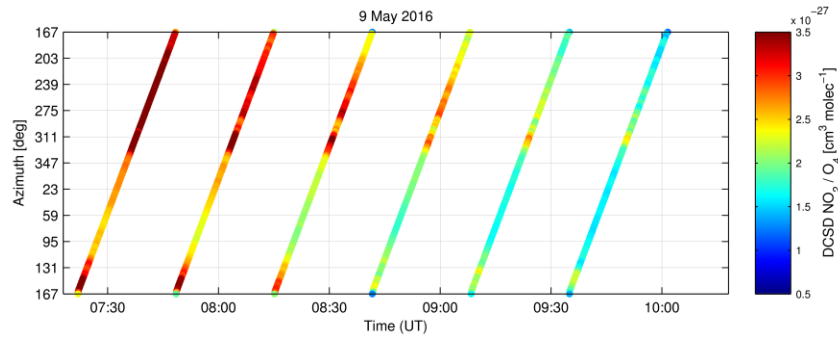
7

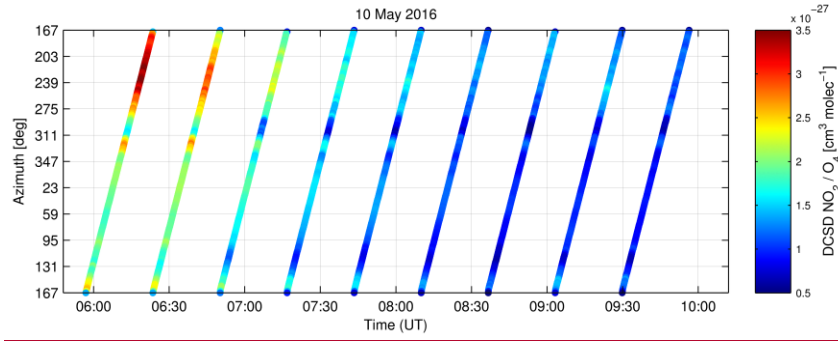


8



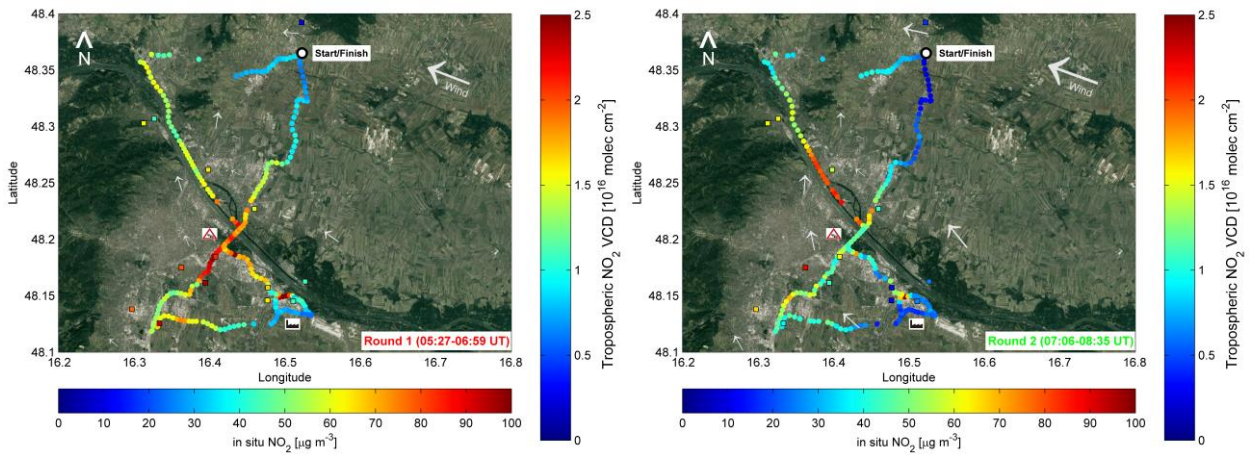
9



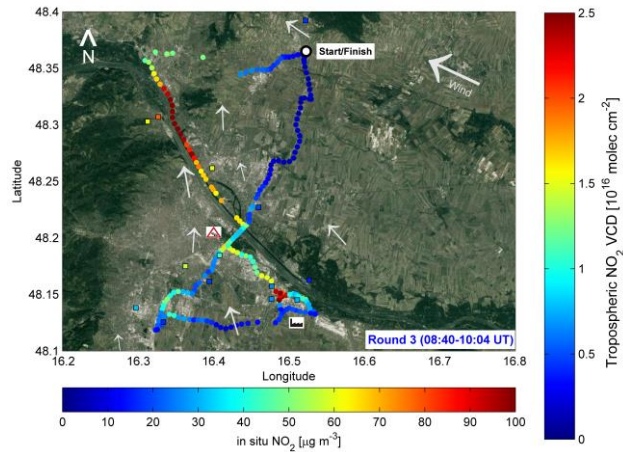


1  
2  
3  
4  
5  
6  
7  
8  
9

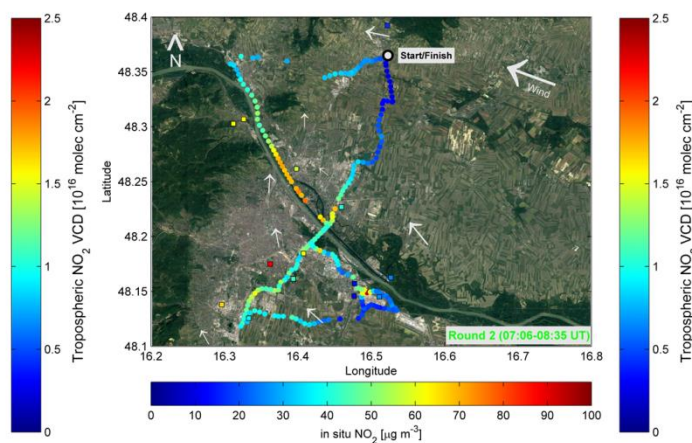
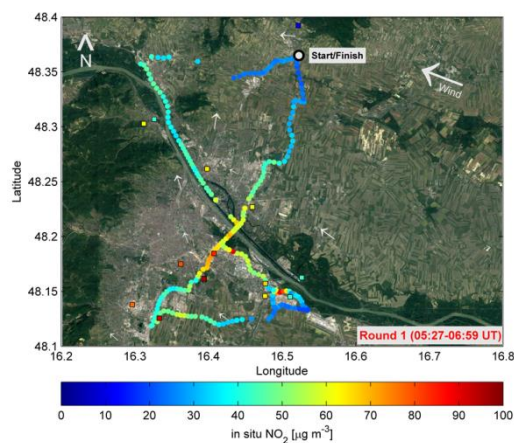
**Figure 1214.** Spatial and temporal variability of DSCD  $\text{NO}_2/\text{O}_4$  obtained from tower DOAS off-axis measurements performed on 9 and 10 May 2016.



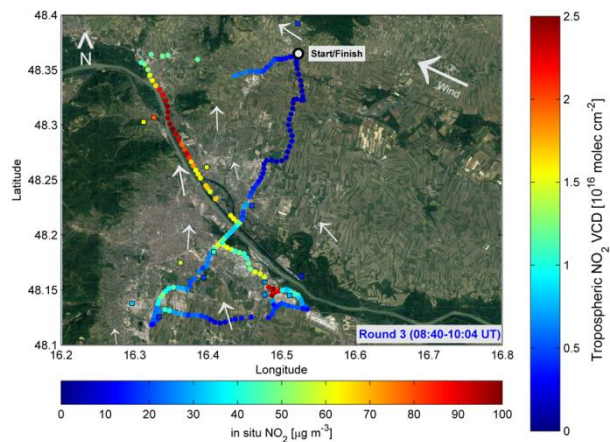
10



1



2



3

4 **Figure 1315.** Spatial and temporal evolution of NO<sub>2</sub> on 10 April 2015 in Vienna as measured by  
 5 the car DOAS zenith-sky (dots) and in situ surface measurements (squares). Wind direction and  
 6 wind speed obtained from local weather stations are indicated by white arrows. The size of the

1 arrows is weighted by the corresponding averaged wind speed (2 m above ground) obtained from  
 2 the individual weather stations. Averaged wind speeds over the course of the car DOAS zenith-  
 3 sky measurements taken on this day ranged between 2.28 and 12.81 km h<sup>-1</sup>.

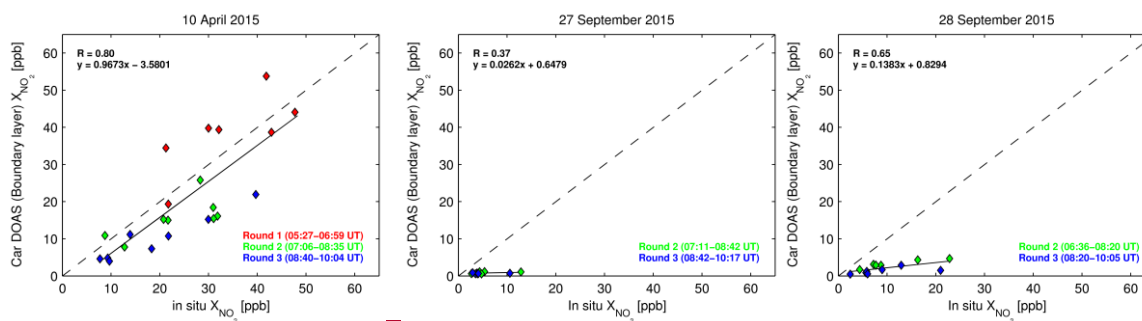
4

5

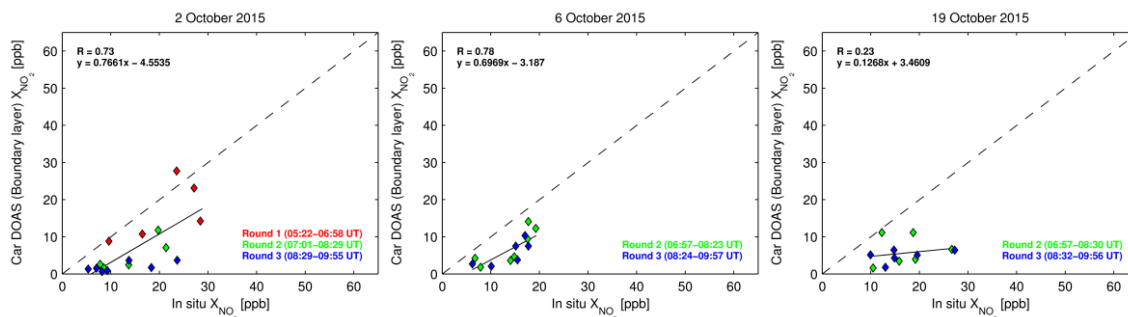
6

7

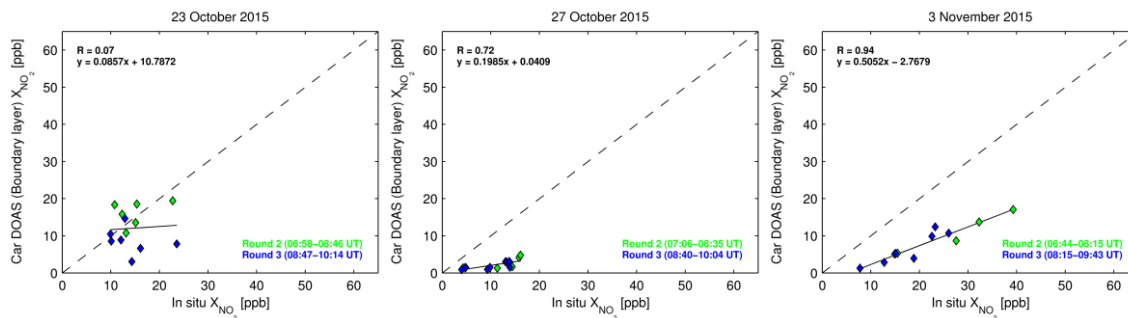
8

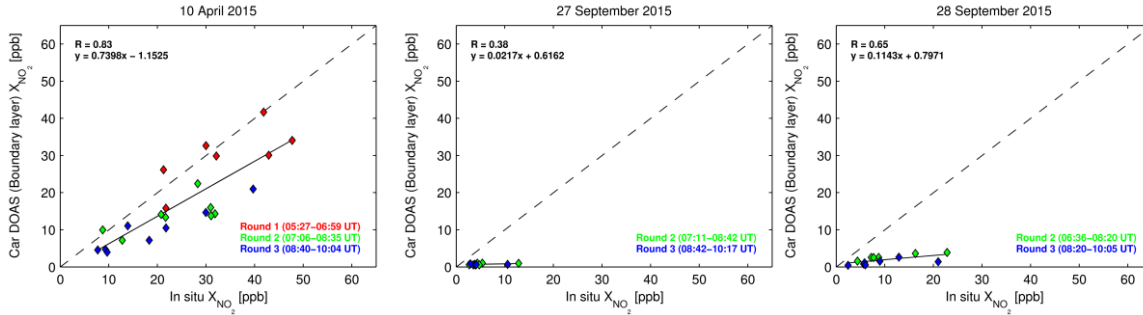


9

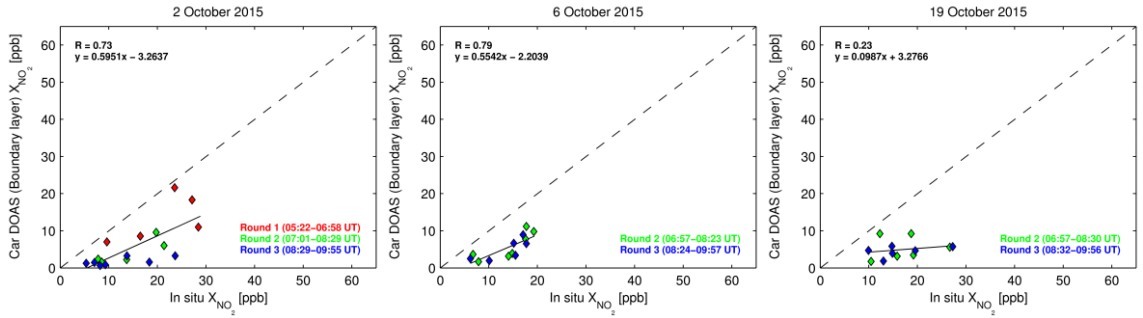


10

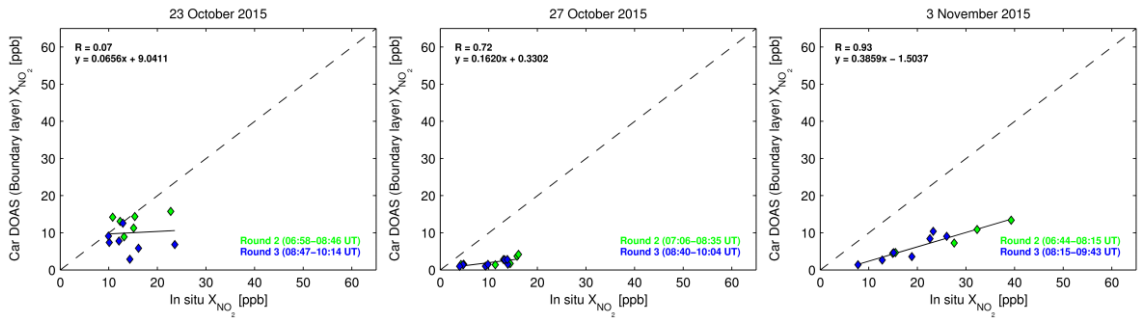




1



2



3

4

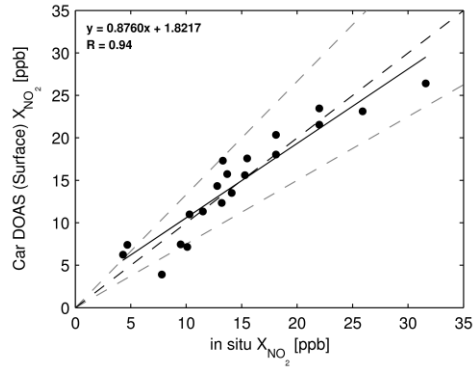
**Figure 1416.** Comparison of boundary layer NO<sub>2</sub> mixing ratios estimated from car DOAS zenith-sky measurements with NO<sub>2</sub> mixing ratios obtained from in situ measurements on the nine days when measurements were performed. The dotted line represents the 1:1 relationship.

7

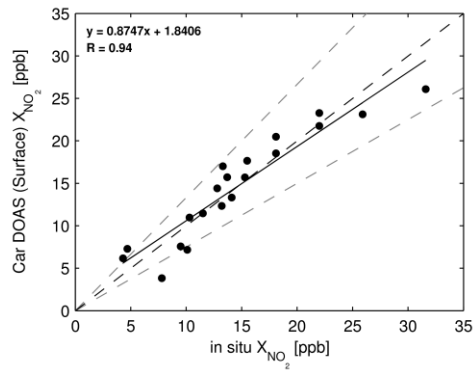
8

9

10



1



2

3 **Figure 1517.** Comparison of lap averaged near-surface NO<sub>2</sub> mixing ratios estimated from car  
 4 DOAS zenith-sky measurements with NO<sub>2</sub> mixing ratios obtained from in situ measurements.  
 5 Lap averages of all twenty performed car rides are included in the calculation. The black and grey  
 6 dotted lines represent the 1:1 relationship and ±25%, respectively.

7

8

9

10

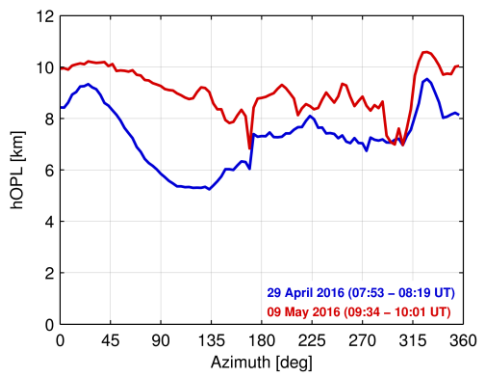
11

12

13

1

2



3

4 **Figure 1618.** Estimated horizontal optical path length obtained from tower DOAS off-axis  
5 measurements recorded during two tower platform rotations on 29 April and 9 May 2016.

6

7

8

9

10

11

12

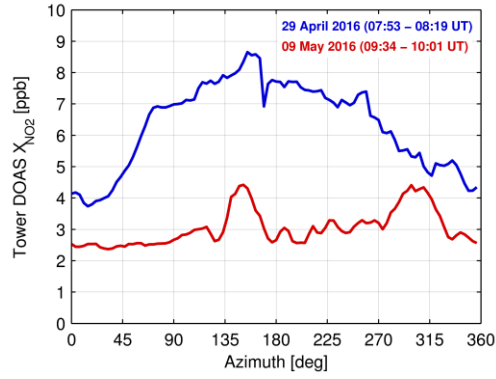
13

14

15

16





1

2 **Figure 1719.** Estimated path-averaged NO<sub>2</sub> mixing ratios obtained from tower DOAS off-axis  
 3 measurements recorded during two tower platform rotations on 29 April and 9 May 2016.

4

5

6

7

8

9

10

11

12

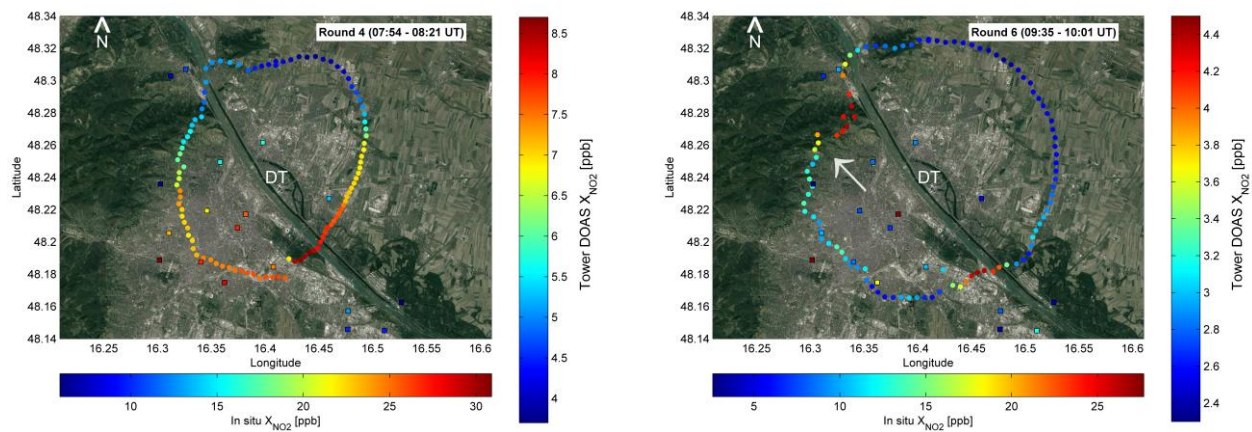
13

14

15

16

17



1

2 **Figure 1820.** Spatial variability of  $X_{NO_2}$  in Vienna based on tower DOAS off-axis (dots) and in  
 3 situ surface measurements (squares) obtained on 29 April and 9 May 2016.

4

5

6

7

8

9

10

11

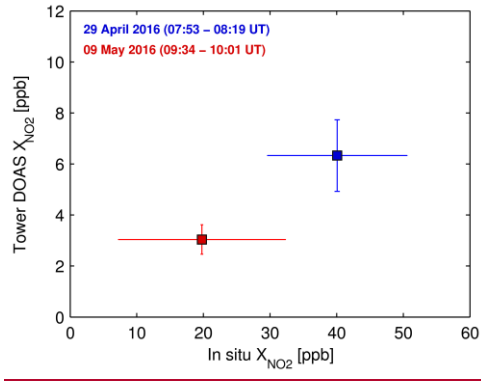
12

13

14

15

16



1  
2 **Figure 21.** Averaged  $X_{NO_2}$  from tower DOAS off-axis as a function of averaged in situ surface  
3  $X_{NO_2}$  on 29 April (blue) and 9 May (red) 2016. The mean and standard deviation of the former is  
4 calculated for round 4 (29 April) and round 6 (9 May) whereas mean and standard deviation of  
5 the latter are calculated from measurements of in situ stations falling within the circle determined  
6 by hOPL of the individual tower DOAS off-axis measurements (see Fig. 20).  
7